Thermo-physical and Mechanical Investigation of Cementitious Composites enhanced with Microencapsulated Phase Change Materials for Thermal Energy Storage

Mona Sam, MSc MSc
Institut für Werkstoffe im Bauwesen, Technische Universität Darmstadt, Germany.
e-mail: sam@wib.tu-darmstadt.de

Antonio Caggiano*, Adj. Prof. Dr. Dr.-Ing.
DICCA – UniGE - Università degli Studi di Genova
Institut für Werkstoffe im Bauwesen, Technische Universität Darmstadt, Germany.
e-mail: antonio.caggiano@unige.it
Deputy Chair of RILEM TC TES:
https://www.rilem.net/groupe/tes-thermal-energy-storage-in-cementitious-composites-422

Liliya Dubyey, MSc
Institut für Werkstoffe im Bauwesen, Technische Universität Darmstadt, Germany.
e-mail: dubyey@wib.tu-darmstadt.de

Jean-Luc Dauvergne, Dr.
Center for Cooperative Research on Alternative Energies (CIC energiGUNE), Basque Research and Technology Alliance (BRTA), Vitoria-Gasteiz, Spain
e-mail: jldauvergne@cicenergigune.com

Eddie Koenders, Prof. Dr.-Ing.
Institut für Werkstoffe im Bauwesen, Technische Universität Darmstadt, Germany.
e-mail: koenders@wib.tu-darmstadt.de

*Corresponding Author: **A. Caggiano** - UniGE - Università degli Studi di Genova antonio.caggiano@unige.it

ABSTRACT

This paper reports a comprehensive experimental investigation of cement pastes enhanced with Microencapsulated Phase Change Materials (MPCMs) for Thermal Energy Storage (TES) purposes. The experimental plan considers three water-to-binder ratios and three MPCM volume fractions, for a total of nine different MPCM paste mixtures. The water-to-binder ratios of the pastes are 0.33, 0.40 and 0.45, which were mixed with a commercial MPCM, namely Nextek 37D® having a melting/solidification temperature of 37 °C, with volume percentage substitutions of 0%, 20% and 40%, respectively. Thermal, physical and mechanical tests were performed to investigate the effect MPCM have on the resulting TES, strengths and conductive properties of the considered mixtures by employing DSC, Hot-Disk, and mechanical tests. The measured latent heat of MPCM was 197.3 J/g and 194.6 J/g for heating and cooling, respectively. The volumetric latent enthalpies for the MPCM-based composites showed an almost constant average of 20-25 MJ/m³ for samples with 20% MPCM and 55-60 MJ/m³ for samples with 40% MPCM, independently of the w/b ratio. Thermal conductivity values measured at 25 and 45 °C ranged between 0.93 to 0.44 W/m×K. Both w/b ratio and MPCM substitution turned out to significantly affect the overall porosity of the composite resulting in a lower thermal conductivity for the MPCM-pastes in comparison to the plain cement matrix. Finally, mechanical tests were conducted that showed a strength loss due to either increasing w/b ratios or for enhanced amounts of MPCM (e.g., up to a 74% and 69% of strength loss were registered for bending and compression, respectively). The thermo-physical and mechanical characterizations were conducted according to an experimental plan that provided a wide set of research results for both sole MPCM and MPCM-cement systems analyzed by SEM, EDS/elemental mapping, contact angle tests, particle size distribution analysis and Mercury Intrusion Porosimetry technique.

KEYWORDS: Thermal Energy Storage, MPCM, DSC, Hot-Disk, SEM, Mechanical Properties, Enthalpy, Latent and Sensible Heat, Heating and Cooling, Porous cementitious paste systems.

1. INTRODUCTION

The energy consumption of the continuously growing building stock is one of the main reasons for the worldwide rise of anthropogenic CO_2 emissions [1]. Cutting back on this cause asks for a major contribution to the sustainable development goals of tomorrow with the aim to make our world carbon neutral. According to recent EU statistics, heating and cooling of buildings represents the biggest single end-use of the EU's building energy consumption (≈ 60% share), where 84% of this energy is still obtained from fossil resources [2]. Moreover, the building energy demand is envisioned to rise by 79% in residential buildings and 84% in commercial ones until 2050 [3]. This scenario is a clear "call-for-action" for the EU, which has committed itself to various ambitious programs to make renovations of residential and non-residential buildings more energy efficient [4].

A smart management of the thermal energy flows from and to a building can hugely contribute to minimize the annual energy consumption by levelling-out the daily and seasonal temperature fluctuations, while enhancing the energy efficiency of the construction as a whole [5][6][7][8]. A very promising technique, to improve the building energy performance in terms of thermal resistance, can be achieved through a smart use of sensible and/or latent TES components, such as Phase Change Materials (PCMs) embedded in cementitious materials [9][10][11].

PCM can be employed to store/release large amounts of thermal energy, predominantly via the latent branch, during melting or solidification at a nearly constant temperature. Ordinary construction materials, like concrete or mortar, only have an intrinsic sensible heat storage capacity, which varies between approximately 0.75 and 1.00 J/g×K [12][13]. In contrast with this, organic PCM can provide excellent latent heat storage capacity of approximately 180-230 J/g [14]. Various researches [15][16][17] demonstrated that passive storage/release of latent heat through phase transformation of PCM from solid-to-liquid or vice versa, can contribute to save considerable amounts of primary energy.

The most appropriate and commercially available PCM for building construction materials are organic compounds since they are chemically stable, safe, non-reactive, do not loss their effectiveness

with cycling, can be microencapsulated and have a wide temperature range [18]. Organic PCM are available in a wide range of materials, including paraffin and non-paraffin (bio-based). The bio-based ones can be (partly) made from renewable resources and have become very popular due to their eco-friendly image for substituting petroleum-based chemicals by bio-based materials [14].

One point of concern when adding PCM in building elements is to avoid (or at least mitigate) a potential leakage during a phase change [19]. Because of this, some techniques have been proposed to integrate PCM directly into the building materials using encapsulations. For example, microencapsulation is considered as one of the most suitable techniques [20] to integrate PCM directly into a composite material [21][22][23]. In this sense, PCM will be microencapsulated (i.e., MPCM) and they mimic a powder-like material, which size typically ranges between 1 μm to 50 μm [24]. They can be easily mixed with the basic cementitious components and have various advantages like a large surface area for heat transfer, are not sensitive to leakage, have a negligible reactivity towards the external environment and allow a clear control of the phase change process [25]. However, although the implementation of MPCM in building composites has been regarded as a good solution to overcome leakage during a phase change, the low thermal conductivity of the encapsulation material (mainly due to the shell thickness) has turned out to be a serious disadvantage for a rapid heat transfer throughout the MPCM and needs improvement [26][27].

Enhancing the energy efficiency of buildings through a successful incorporation of MPCM in cement-based composites requires more in-depth research [28][29][30][31][32]. Especially drawbacks like shrinkage, or the unsatisfying thermal conductivity of encapsulation material, needs to be comprehended before larger amounts of MPCM can be incorporated in a mixture [33]. Therefore, to produce stable MPCM-cementitious composites, it is of key importance to study mix designs with different MPCM dosages (especially high-volume percentages) and different (from low-to-high)) water to binder (w/b) ratios. In this regard, there is a clear need to further investigate the thermal and mechanical behaviour of cement pastes enriched with MPCM while varying a number of factors, such

as *core/shell* type and *core size/shell thickness ratio* of MPCM, type of fillers and supplementary components, as well as the mixing procedure. Available studies have already been addressed, which, from an experimental point of view, emphasized the hygro-thermo-chemo-mechanical properties of cement-based materials containing MPCM at several length-scales and applications [34][35]. In these studies, common techniques like Differential Scanning Calorimeter (DSC) [36], Differential Scanning Calorimetry (DSC) and Scanning Electron Microscopy (SEM) [37] have been employed, where the thermo-physical properties of MPCM-cementitious composited were investigated.

Only a few studies available in literature address the importance of MPCM properties once embedded in cementitious composites [38][39]. For instance, Cao et al. [40] pointed out that the early stage viscosity is much more affected by MPCM with a hydrophilic surface than those with a hydrophobic one. Furthermore, Coppola et al. [41] described that by increasing amount of MPCM, from 5% to 20% by weight of substituted binder, the workability of paste will be greatly affected, leading to an increased water demand of a mixture. In addition, Sanfelix et al. [42] compared the polarity effect of MPCM shells on the flowability of cement paste and concluded that a Melamine-Formaldehyde (MF) based shell had most suitable rheological properties. It may be worth to mention that the majority of studies showed only limited additions of MPCM, viz. up-to 20 wt% [43][44][45]. Therefore, the main novelty of this paper is on the impact of high amounts of MPCM (up-to 40 %) on the properties of cementitious composites by examining the influence of hydrophobic MF shells on the porosity, strength, and thermal-energy storage, i.e. heat capacity and conductivity.

In the present work, results of a detailed experimental program are reported, investigating the thermal behavior of cementitious composites containing MPCM. The thermal analyses were performed by considering DSC measurements and Hot-Disk conductivity tests. The tests were aimed at quantifying the sensible and latent heat storage for cement pastes, MPCM and MPCM-paste systems. Three water-to-binder ratios and three MPCM volume fractions, for a total of nine mixtures, were analyzed. The thermal energy storage study is accompanied by mechanical and other physical tests (including SEM

analyses, MPCM contact angle tests, MPCM particle size distribution analysis, MIP and EDS/elemental analysis) to completely investigate the considered MPCM cement paste systems.

2. MATERIALS AND METHODS

This section is reporting the Materials and Methods adopted for investigating the properties of components and composites of the experimental study. Samples for thermal, mechanical and physical analyses were cast and tested for investigating both plain and MPCM-cement pastes.

2.1. Materials and mixtures

A Portland cement CEM I 52.5R [46] with a density of 3.10 g/cm^3 was used. In order to reduce the environmental impact of the cement, an eco-friendly metakaolin binder (namely Centrilit NC II made of reactive aluminosilicate pozzolan [47]) was also used as partial substitute of the CEM I 52.5R. The chemical composition of both binders is listed in ***Table** 1*.

Energy efficiency in buildings is strongly affected by the ability of insulation materials to (partly) block the outer heat flux. High performance insulation materials are nowadays under development showing a high energy-efficiency while covering all weather and climates. New research directions are dealing with dynamic temperature-adaptable building envelopes, which are applicable in either cold or hot climates. From this, cement-based composites made with MPCMs having melting/solidification temperatures beyond the standard thermal comfort range (i.e., 19 °C and 26 °C) have to be investigated on their potential to be used in TES applications of construction and building materials. For this reason, in this manuscript MPCM-composites with a melting/solidification temperature of 37 °C have been investigated while representing hot temperature climates. Thus, paraffin-based MPCM were evaluated, namely Nextek 37D® (labelled as N-MPCM) provided by Microtek Laboratories [48]. N-MPCM is composed of a paraffin-mixture core and a melamine-formaldehyde polymer shell (MF) and its main properties are outlined in *Table 2*.

***Table** 1: Overview chemical composition of cement (CEM I 52.5 R) and* Metakaolin (Centrilit NC II*).*

Chemical composition [% weight]	*SiO_2*	*Al_2O_3*	*Fe_2O_3*	*CaO*	*MgO*	*Na_2O+K_2O*
Cement CEM I 52.5 R	***20.10***	*4.50*	*3.30*	***64.90***	*1.40*	*0.93*
Metakaolin	***52.1***	***41.0***	*4.32*	*0.07*	*0.19*	*0.89*

Table 2: Thermo-physical properties of Nextek 37D® N-MPCM [48].

Properties	***N-MPCM***
Core	*Paraffin mix*
Shell	*Melamine Formaldehyde (MF)*
$T_{m,\,peak}$ [^oC]	*37*
Density [g/cm^3]	*0.76*
Latent heat capacity [J/g]	*190-200*
Mean particle size [µm]	*15-30*

Table 3: Mix overview of the nine paste systems.

Labels	***S-45-ref [kg/m^3]***	***S-45-20 [kg/m^3]***	***S-45-40 [kg/m^3]***	***S-40-ref [kg/m^3]***	***S-40-20 [kg/m^3]***	***S-40-40 [kg/m^3]***	***S-33-ref [kg/m^3]***	***S-33-20 [kg/m^3]***	***S-33-40 [kg/m^3]***
w/b ratio		***0.45***			***0.40***			***0.33***	
Cement	*983.4*	*786.7*	*590.0*	*1043.1*	*834.5*	*625.8*	*1140.0*	*912.0*	*684.0*
Metakaolin	*161.8*	*129.4*	*97.1*	*171.6*	*137.3*	*103.0*	*187.6*	*150.1*	*112.5*
Water	*515.3*	*412.3*	*309.2*	*485.9*	*388.7*	*291.5*	*438.1*	*350.5*	*262.8*
Superplasticizer	*5.7*	*4.6*	*3.4*	*6.0*	*4.8*	*3.6*	*6.6*	*5.3*	*3.9*
Stabilizer	*33.1*	*26.5*	*19.8*	*35.1*	*28.0*	*21.0*	*38.3*	*30.7*	*23.0*
MPMC [V.-%]	*-*	*20*	*40*	*-*	*20*	*40*	*-*	*20*	*40*
Hardening accl.	*22.9*	*18.3*	*13.7*	*24.3*	*19.4*	*14.5*	*26.5*	*21.2*	*15.9*

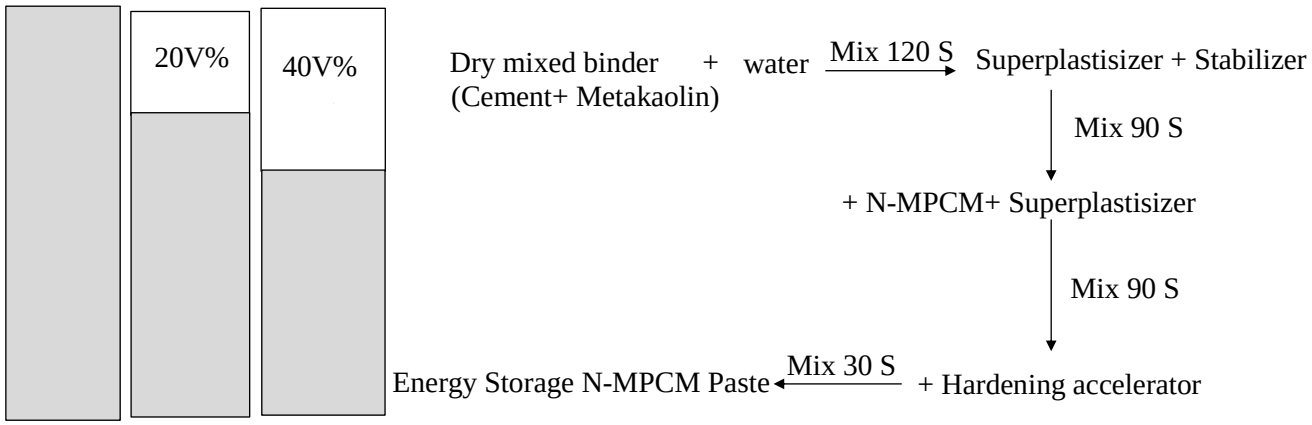

(a) (b)

Figure 1: Cement pastes: (a) N-MPCM volume fractions and (b) mixing procedures.

Nine N-MPCM-cement mixtures were considered which were made with three different water-to-binder (w/b) ratios and 3 amounts (0, 20% and 40%) of N-MPCM volume fractions. All mixtures have been prepared following the casting procedure of EN 196-1 [49] and the recipes of *Table 3*. The table's first row indicates the label of the mixture highlighting the necessary information on the considered w/b ratio along with the amount of N-MPCM (expressed in % of paste substitution, see *Figure 1*). For example, ''S-45-20'' refers to a mixture having a w/b=0.45 and 20% of N-MPCM volume fraction.

After making different trials of mixing procedures, the order of component addition and mixing conditions were optimized as follows. First, cement and metakaolin were hand-mixed until a homogeneous appearance was achieved. Then, the binder was mixed with water for 120 s followed by a superplasticizer and mixed for another 60 s until the appropriate workability of the mixture was reached. The stabilizer was added to the mixture for further 30 s. At this point, for the reference pastes (without N-MPCM) the hardening agent was added and mixed for another 30 s, after which the paste was immediately poured into the moulds. For mixtures with N-MPCM, the procedure was optimized by considering again the workability of the paste, mixing the N-MPCM with the cement paste for an additional 90 s, during which mostly extra superplasticizer was added. The procedure was finished by adding the hardening agent and mixing it for a final 30 s.

The batch volume was calculated to produce at least 3 prisms of 40 mm × 40 mm × 160 mm (employed for mechanical testing and microstructure/porosity measurements), two cylindrical samples of 20 mm high and 56 mm of diameter, needed for the hot-disk measurements, and three crucibles for DSC analyses. One day after casting, all the specimens were demoulded and stored in a water bath at 20° C, until 28 days. Subsequently, mechanical tests were performed. DSC and thermal conductivity measurements, were also conducted with specimens that were stepwise dried at 30° C, 40° C and 50° C until they reached a constant mass.

2.2. Methods

2.2.1 N-MPCM

Characterization of N-MPCM was performed by evaluating the particle size distribution, shell polarity with contact angle measurements, as well as morphology with SEM analyses.

Particle size distribution

To determine the mean particle size of the N-MPCM, laser granulometry (Partica LA-950 Laser Diffraction Particle Size Distribution Analyzer) was used. It works according to the following principle: a laser is scattered by a group of particles. The angle of light scattering is inversely proportional to particle size. The diffraction patterns of different particle diameters are well known. So, a mathematical algorithm based on the Mie theory is used to compute the portion of the theoretical spectra of all particle size classes from the experimentally determined total spectrum. The complex refractive index of the particle is needed by employing the Mie theory. With the knowledge about the N-MPCM shell material, it is possible to know the refractive index and to perform this measurement. Considering that N-MPCM is essentially made of melamine-formaldehyde, the refractive index value taken from the literature was 1.68 [50].

Contact angle measurement

One of the aims of this work is also to investigate the influence of the N-MPCM shells on the surrounding microstructure of the cementitious composite. Therefore, the measurement of the contact angle is of key importance in this sense because it is one of the most practical parameters to effectively characterize the hydrophilic/hydrophobic nature of a material surface.

The contact angle is a measure between the liquid-solid and the vapor-liquid interfaces (namely, where the vapor-liquid interface tangent line from the point of intersection of the liquid, solid, and vapor phases meet, “three phase contact point”, along with the vapor-liquid interface of the droplet).

This is a balance of three equilibrium interfacial tensions that follows equation [51]:

$$\gamma_{LG}\cos\theta = \gamma_{SG} - \gamma_{sL} \quad (1)$$

where θ is the contact angle and γ_{LG}, γ_{SG} and γ_{SL} represent the liquid-vapor, solid-vapor, and solid-liquid interfacial tensions, respectively. Surfaces with a higher tendency to absorb water molecules possess a contact angle lower than 90˚ and are defined as "hydrophilic". On the contrary, surfaces with less affinity towards water are so-called "hydrophobic", showing a contact angle higher than 90˚ and they tend to reject water molecules. To determine the water affinity of N-MPCM, the contact angle was measured using the Contact Angle (CA) goniometer (OCA instrument: *DataPhysics Instruments, Filderstadt, Germany*). A static Milli-Q water droplet with a volume of 3 ul was placed on the sample. The CA was determined via Young–Laplace alignment 1 s after drop generation.

2.2.2 N-MPCM-cementitious pastes

The characterization methods employed to investigate the mechanical, thermal and physical properties of the designed pastes are presented in this section.

Differential Scanning Calorimeter (DSC)

The DSC 214 Polyma equipment was used to perform the DSC studies on the either with or without N-MPCM cementitious pastes. DSC is a thermo-analytical technique that measures released (exothermic) and absorbed (endothermic) heat with varying temperatures. It is a commonly used technique to determine heat capacities, melting peaks, and enthalpies of PCM, N-MPCM, as well as N-MPCM-enhanced composites. The samples were prepared in aluminum DSC crucibles (*Figure 2*a), cured until 28 days, and oven-dried at 50 ºC until a constant weight was achieved. The crucibles have a diameter of 6 mm and a maximum volume capacity of 40 µl. A small hole (*Figure 2*b) was made in their lid to enable isobaric measurements.

The German Standards DIN 51005 and DIN 51007 [52][53] were considered as a reference to perform the DSC tests, while the IEA standard procedure [54] was followed to determine the latent heat storage capacity of N-MPCM-composites. The thermal program used included a temperature interval

from 15 ºC to 45 ºC (for heating and cooling), considering that the melting temperature of the N-MPCM is around 37 ºC. Each measurement included three cycles of heating and cooling, with an isothermal 10-minute section to ensure that the thermodynamic equilibrium is attained. All measurements were done under an inert nitrogen environment at a flow of 60 ml/min. The measurements for the paste with N-MPCM were done at a rate of 0.5 K/min and for reference pastes at a rate of 10 K/min.

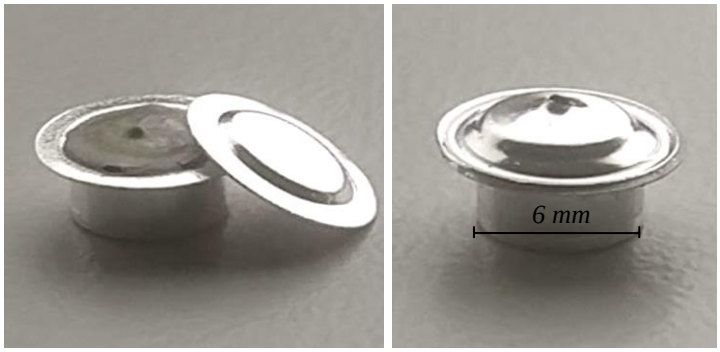

(a) *(b)*

Figure 2: (a) aluminum sample holders (maximum volume capacity of 40 μL) and (b) prepared sample inside crucible with a small hole on top.

Mechanical tests

To characterize the mechanical response of the N-MPCM cement pastes prismatic samples were tested following the procedures described in EN 196-1 [49]. For each mixture with the commercial N-MPCM, 9 prisms (40 mm × 40 mm × 160 mm) were prepared and tested after 3, 7, and 28 days. Three identical samples per each mixture/maturation were considered which were firstly tested under a three-point bending scheme. The distance between the bending supports was 100 mm (± 0.5 mm) and the vertical load was imposed with a loading rate of 50 N/s until failure. Then, compression tests were performed by employing one half of a broken beam.

The bending strength R_f of all mixtures was calculated by means of the following expression [49]:

$$R_f = \frac{1.5 \cdot F_f \cdot l}{b^3} \quad (2)$$

where *b [mm]* is the rib size of the beam cross-section, F_f *[N]* the applied load and *l [mm]* the distance between the end supports. The compressive strength was determined according to the following formula:

$$R_c = \frac{F_c}{A_c} \tag{3}$$

being F_c *[N]* the failure load and A_c the area of the auxiliary plates (40×40 mm^2).

Mercury intrusion porosimeter (MIP)

MIP tests (as shown in *Figure 3*) were executed to better understand the changes in the pore structure of the considered composites. Pore structure plays a major role in both mechanical and thermal properties of cement pastes.

(a) *(b)*

Figure 3: a) Sample holder together with Specimen Fractures tested under MIP and b) Mercury intrusion porosimeter Thermo Scientific Pascal 140 and 440.

Mixtures with higher w/b ratios are expected, not only to have lower compressive strengths, but also to have higher pore volumes and larger critical pore diameters. Moreover, the addition of N-MPCM might also affect the pore structure by reducing the hydration degree and rate, which keeps pores larger and free of hydration products.

The Washburn equation, which assumes a cylindrical pore shape, is used to analyze MIP results [55]. The pore size detected is influenced by two factors: the surface tension of mercury (γ) and the contact angle between the mercury and the pore surface (θ). The latter evaluates the pore size as follows:

$$D = \frac{4\gamma cos\theta}{P} \quad (4)$$

Morphological and elemental analysis via SEM

Scanning Electron Microscopy (SEM) analyses were performed for N-MPCM cement pastes to investigate microscopic properties of composites in terms of geometry, shape, particle size, and particle distribution. For this purpose, the analysis can shed information on the following characteristics:

- Homogeneous distribution of N-MPCM;
- Integrity of shell structures of N-MPCM;
- Particle size and uniformity of N-MPCM;
- Thermal and mechanical stability of microcapsules;
- Effect N-MPCM have on the microstructure of the cementitious composite.

The microstructure of the cementitious samples was observed through an Atmospheric scanning electron microscope (Zeiss EVO LS25) after 28 days of curing. The samples were cut into approximately 2×2×2 cm^3 and placed in cylindrical molds as shown in *Figure 4*. For sample preparation, vacuum impregnation was used to embed the samples in an epoxy mixture (i.e., 25 g of epoxy to 3 g of hardening accelerator). Afterward, the surface was polished with a Lab polishing device. All samples were visualized at an accelerating voltage of 15 kV. Back-scattered-electrons (BSE) mode and Second Electron (SE) mode were used to obtain good contrast between the microcapsules and the cementitious matrix, as well as the topographic analysis, respectively.

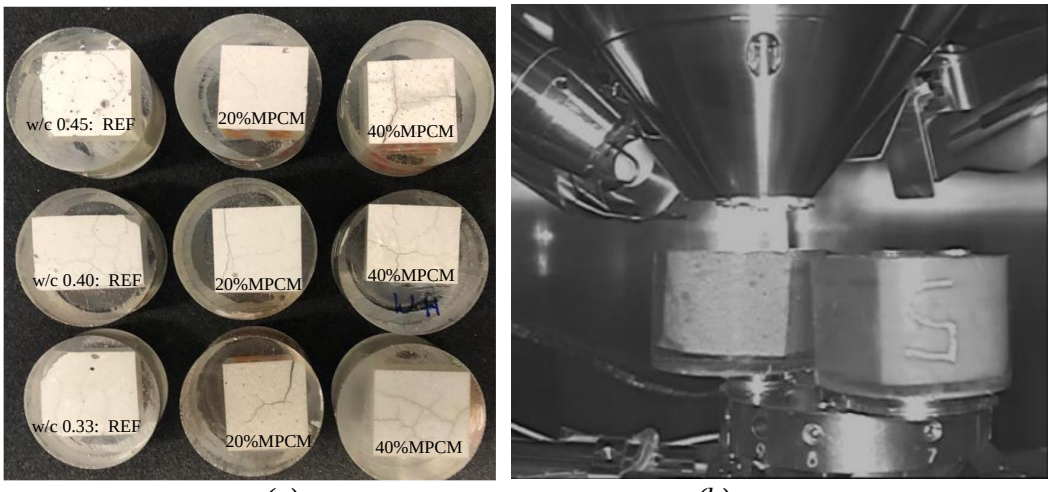

(a) *(b)*

Figure 4: a) 2×2×2 cm^3 cement paste samples being impregnated and polished and b) samples inside the vacuum chamber being tested under SEM.

Elemental analyses of samples were accomplished by using Energy-Dispersive X-ray spectroscopy (EDX) while elemental mappings were performed in low vacuum mode (at 10 Pa) with a voltage of 15 kV, beam current of 2.0 nA and an EDX detector (EDAX, Ametek, Berwyn, PA, US).

Hot Disk TPS Thermal conductivity

The assessment of the effective thermal conductivity was performed by means of the Transient Plane Source (TPS) method, known as Hot-disk following the norm Hot Disk ISO 22007-2:2015. Upon 28 days of curing, two cylindrical samples (56±1 mm diameter and 25±1 mm thickness) (see *Figure 5*a) of each mixture were analyzed.

This method is based on the use of a transiently heated plane sensor sandwiched between two samples of the material to be characterized (see *Figure 5*a). The measurements were done with a Kapton 5501 sensor (6.403 mm) (see *Figure 5*c), inside of a climatic chamber at 10 ºC below and above the melting point of the incorporated N-MPCM during 40 s, and for reference samples at 20 °C during 80 s, both with a heating power of 80 mW.

(a) *(b)* *(c)*

Figure 5: a) Test set-up for the TC measurement b) Cured sample prepared for the TC measurement and c) and Hot Disk Kapton 5501 sensor.

315 Relative humidity was fixed at 60 % RH for all the experiments. At least 3 measurements were
316 carried out for each sample by moving it between each test, and the recorded data were processed using
317 the Hot Disk Software (version 7.4.0.10).

3. RESULTS AND DISCUSSION: N-MPCM

3.1. Morphology of the N-MPCM

Particle size of N-MPCM was investigated through size diffractometer measurements, while their visual appearances were verified through SEM analyses. In this sense, *Figure 6* (a) plots the cumulative and discrete size distribution of the N-MPCM, while *Figure 6* (b) shows the physical appearance of the capsules. The N-MPCM presents a mean particle size of 20.9 µm: this result is also confirmed by SEM visualization and diameter measurements of a single capsule. It is then observed that N-MPCM has a low tendency to agglomerate, confirmed by the almost absence of large shaped spheres (*Figure 6*b) which is often caused by particle grouping.

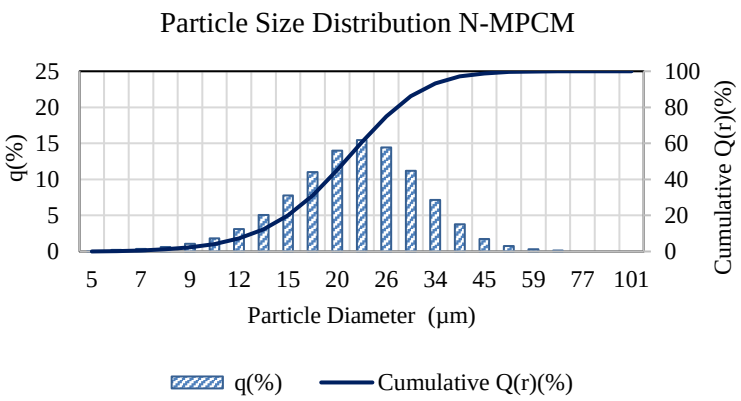

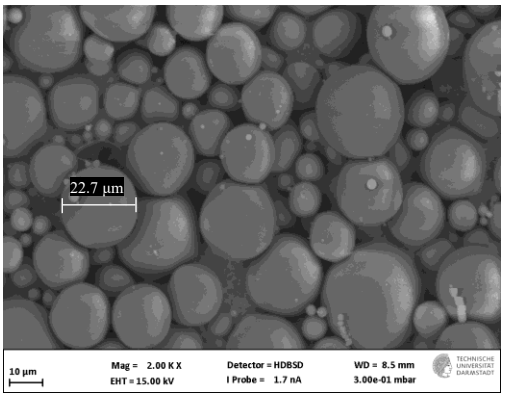

(a) *(b)*

Figure 6: (a) cumulative (solid line) and discrete (histogram bars) particle size distribution of N-MPCM and (b) SEM visualization of pure Nextek 37D® MPCM.

The wettability of the N-MPCM microcapsules was assessed with contact angle measurements which results are presented in *Figure 7*. The sub-Figure a) marked with a blue square box shows the moment in which the drop got attached to the base support where the angle is experimentally measured. The test was performed 10 times in different parts of the tape and the mean value was determined. It was experimentally observed that the droplet on N-MPCM capsules was relatively static, after being dropped,

without being absorbed into the sample. This deals with the hydrophobic nature of the N-MPCM microcapsules. Particularly, the results show that the N-MPCM contact angle presents an average of 110.7 º. Hence, reminding that the higher the contact angle the more hydrophobic is the sample, it can be concluded that the N-MPCM is characterized by a clear hydrophobic microencapsulation. This is an important finding to take into consideration for the stability/performance of cementitious composites made of mixing pastes and N-MPCM microcapsules.

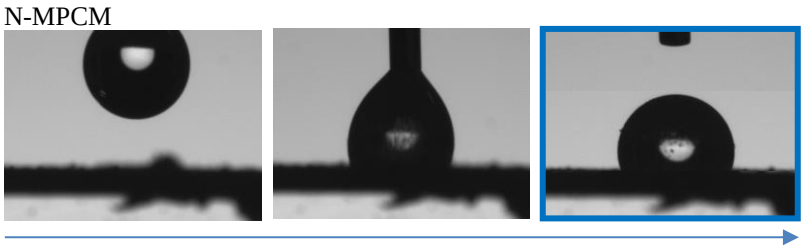

(a)

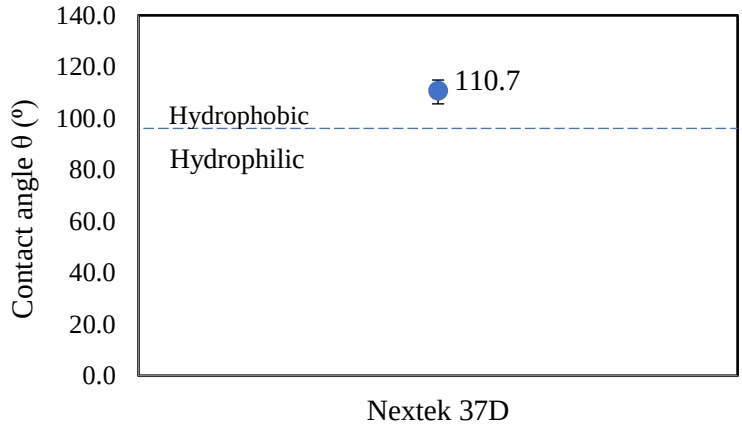

(b)

Figure 7:(a) Contact angle measurement of N-MPCM and (b) Average value among 10 measurements.

3.2. Thermal properties of the N-MPCM

To investigate the latent heat performance of the selected N-MPCM, DSC measurements were performed on the powder-like N-MPCM. Samples of around 10 mg were considered for the DSC-measurements, while three samples with three periodic cycles of heating/cooling by considering a heating/cooling rate of 0.5 $K \times min^{-1}$ were investigated. The chosen heating/cooling rate was experimentally determined to provide a negligible influence on the heating/cooling peak of the final DSC curves [14]. The record of the *DSC* curves is expressed in terms of heat flow versus temperature. From these results, the specific heat capacity and latent enthalpy of the N-MPCM was subsequently calculated (see *Figure 8* a and b, respectively).

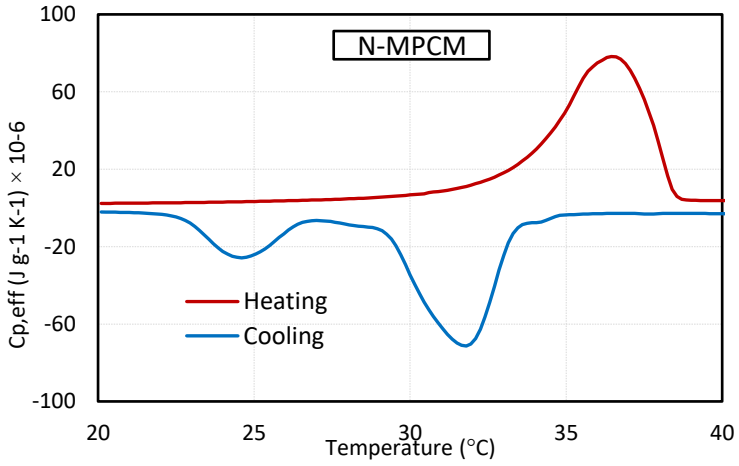

(a)

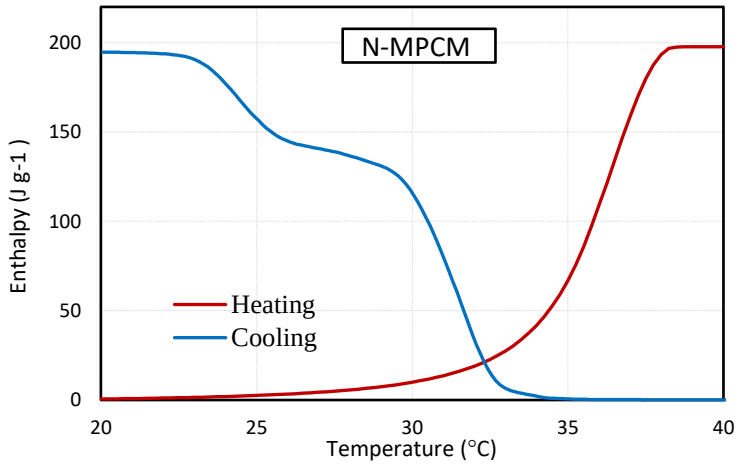

(b)

Figure 8: Results of DSC measurements of pure N-MPCM obtained with a heating/cooling rate of 0.5 K / min (a) $C_{p,eff}$ versus T for heating and cooling between 20 °C and 40 °C (b) latent heat storage (enthalpy) in the melting Temperature range of pure N-MPCM.

Figure 8 shows the results of DSC measurements expressed as $C_{p,eff}$ versus T. The thermographs show that the shape of the curves is quite similar for heating and cooling where a clear one-peak response can be observed for heating, while two peaks characterize the cooling. This suggests that the N-MCPM has a tendency for subcooling. However, despite the differences in the heating/cooling peaks and shapes they did not have influence the total melting/freezing enthalpy.

The applicable melting temperature range (under heating) of the N-MPCM starts at 33.4 °C and reaches the peak at 36.5 °C. Under cooling cycle, the solidification starts at 33.3 °C and reaches its peak at 31.7 °C. The values of the latent heat obtained for N-MPCM is 197.3 J/g and 194.6 J/g, for heating and cooling, respectively (see Table 4). The latter coincide within the range of 190-200 J/g as provided by the provider´s data sheet [48].

Table 4. Results from DSC measurements of N-MPCM, with a heating/cooling rate of 0.5 k/min.

		$T_{transition,\ onset}$ [°C]	$T_{transition,\ peak}$ [°C]	Latent heat [J/g]
Heating	*N-MPCM*	*33.4*	*36.4*	*197.3*
Cooling	*N-MPCM*	*33.3*	*31.7*	*194.6*

4. RESULTS AND DISCUSSION: N-MPCM-PASTES

This section aims at providing an extensive characterization of the thermo-physical properties of the designed cementitious systems with and without N-MPCM incorporation.

4.1. DSC results

4.1.1 Reference pastes

DSC results of the three reference cement pastes, with a w/b ratio of 0.45, 0.40, and 0.33, were examined. The DSC measurements were carried out with a heating/cooling rate of 10 K/min and the effective heat capacities are shown in *Figure 9*. The thermal storage performance of the three different cement pastes, over the entire examined temperature range from 5 °C to 40 °C, is characterized by an exclusively sensible TES behavior.

As it can be appreciated from the curves obtained, there is an almost identical behavior for all pastes. When comparing the heat capacity per unit of mass (*Figure 9*-a), the paste "REF w/b 0.45" has a slightly increased heat storage capacity compared to either "REF w/b 0.40" or "REF w/b 0.33". However, in terms of volumetric heat capacity (*Figure 9*-b), it can be seen that the order changes, having "REF 0.33" a slightly higher storage capacity than "REF 0.45" and "0.40". This fact is due to the higher bulk density of the REF 0.33 paste with the calculated dry density of 1824 kg/m³ and the measured dry density of 1702 kg/m³, in contrast to lower values for "REF 0.45" and "REF 0.40" (see Table 5). Furthermore, the results also show a typical temperature dependence of the heat storage capacity with a slightly increasing trend at higher temperatures.

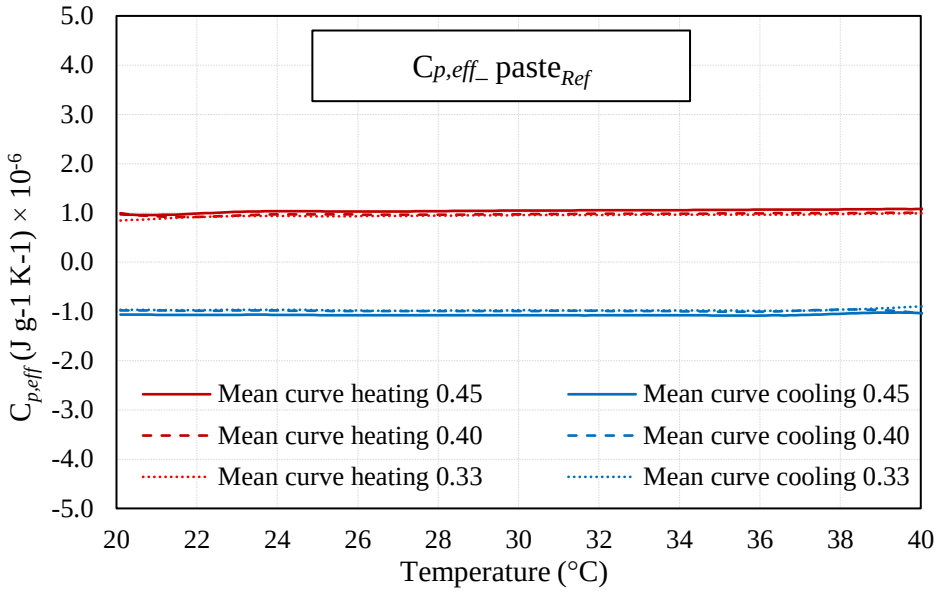

a)

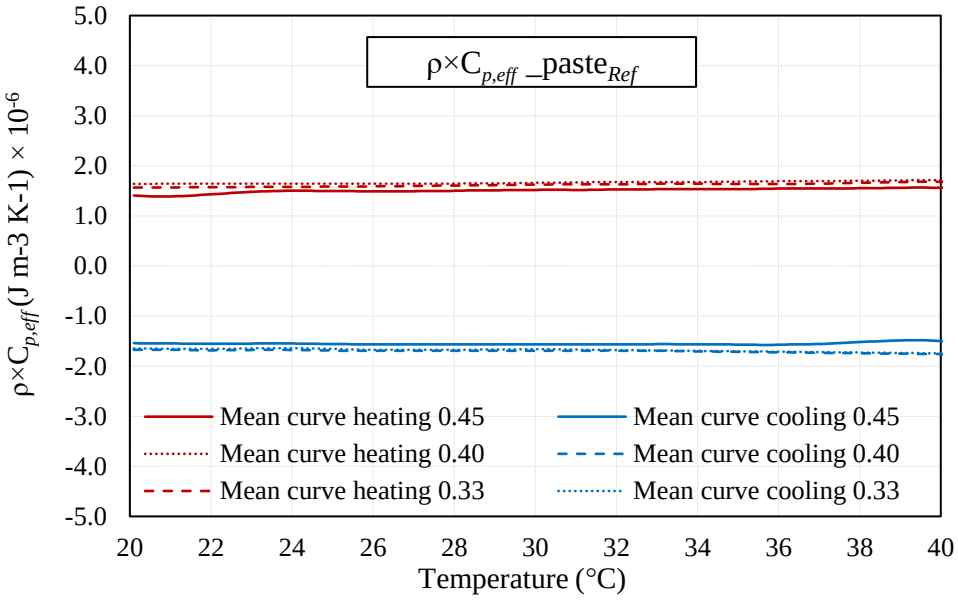

b)

Figure 9: DSC results of the pastes (w/b=0.45, 0.40 and 0.33): a) C_p vs *T and b) $\rho \times C_p$* vs *T.*

*4.1.2 Cement paste with **N**-MPCM 20 vol.-% and 40 vol.-%*

Analogous to the measurements of the pure N-MPCM, a heating rate test was carried out prior to the measurements for the N-MPCM-pastes. This was necessary to fulfill the requirements of the IEA-SHC 42 Standard (see [14] and [54]): the proper heating/cooling rate which ensured the required

thermal equilibrium within the sample, during the measurements, was found to be 0.5 K/min. Therefore, all measurements were carried out under the heating/cooling rate of 0.5 K/min while three different samples for the same mixture design were tested, each within three identical heating/cooling cycles. *Figure 10* (a) and (b) show the average $C_{p,eff}$ curves obtained from the DSC-measurement results. To ease comparability of the results, and because of the volumetric substitution of N-MPCM in cement matrices, also the graphs regarding the volumetric heat capacity ($\rho \times C_{p,eff}$) are presented, see *Figure 10* (c) and (d) . In order to calculate the volumetric heat capacity ($\rho \times C_{p,eff}$), the paste densities ρ were taken from the conducted MIP results (more details are available in Section 4.4) and presented in Table 5.

Table 5. Paste densities *with and without N-MPCM* measured via Heliumpyknometer.

ρ (g/cm3)	*0.45ref*	*20% 0.45*	*40% 0.45*	*0.40ref*	*20% 0.40*	*40% 0.40*	*0.33ref*	*20% 0.33*	*40% 0.33*
N-MPCM	*1.450*	*1.332*	*1.126*	*1.708*	*1.438*	*1.221*	*1.702*	*1.584*	*1.242*

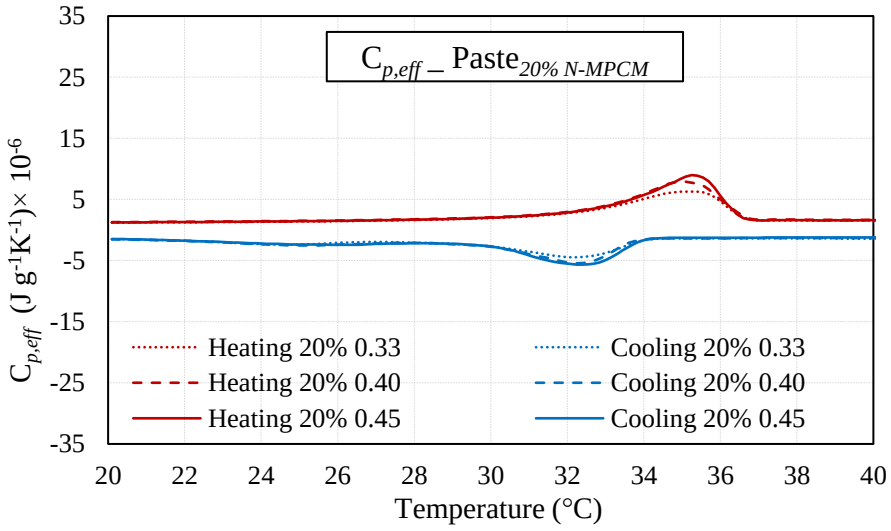

(a)

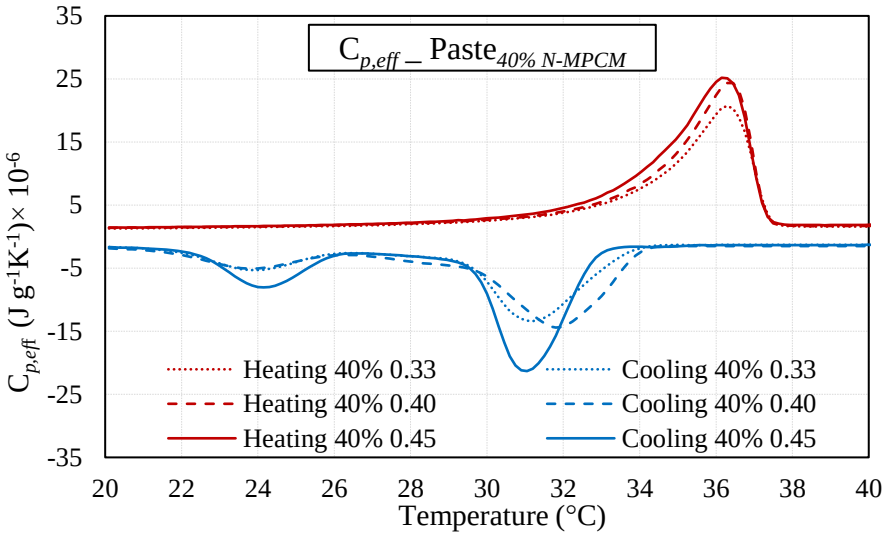

417

418 *(b)*

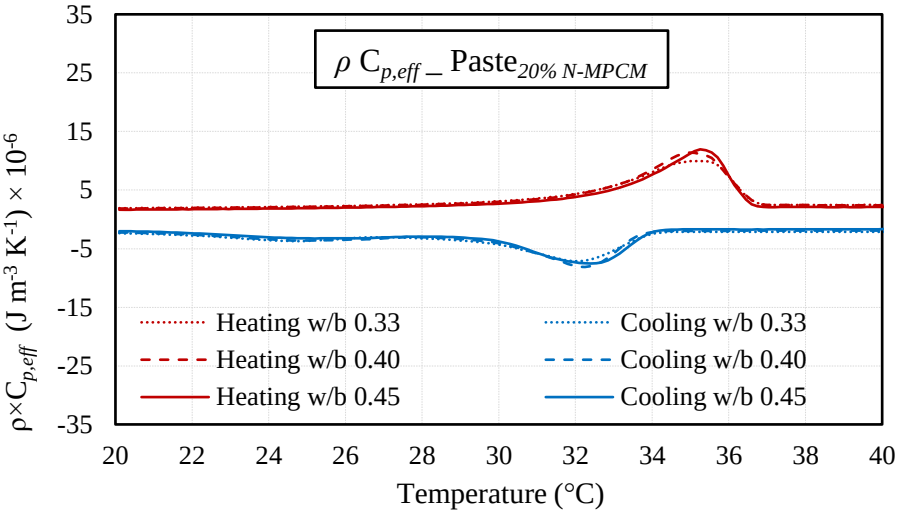

419

420 *(c)*

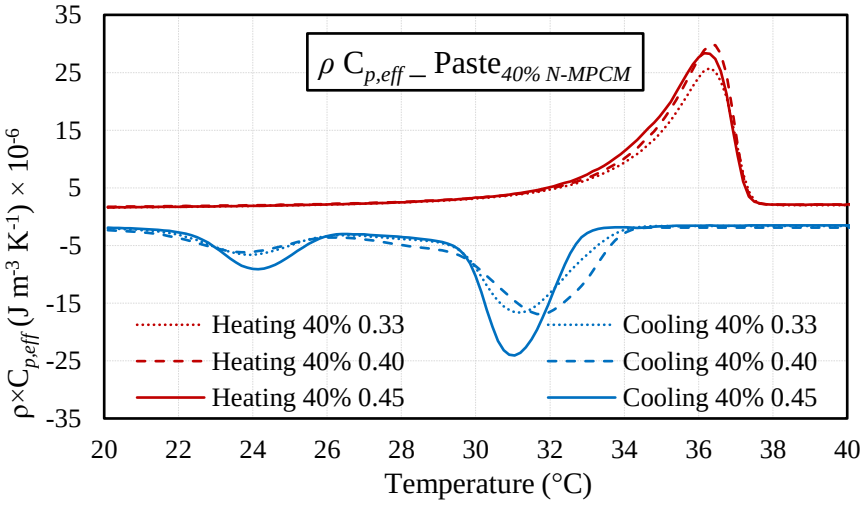

421

422 *(d)*

423 *Figure 10: DSC results- (a) $C_{p,eff}$ of 20% and (b) 40% N-MPCM pastes (w/b=0.45, 0.40 and 0.33).*

424 *(c) ρ×$C_{p,eff}$ of 20% and (d) 40% N-MPCM pastes (w/b=0.45, 0.40 and 0.33).*

From the plotted graphs in *Figure 10*, the melting onset temperatures (i.e., Onset temp.), the peak temperatures (Peak temp.) and the latent heat capacities have also been listed in Table 6. The graphs of *Figure 10* and the values of Table 6 show that the w/b ratio does not significantly influence the thermal behavior of the N-MPCM enhanced cementitious composites. The lowest onset temperature for heating was 32.2 °C while the highest one (upon cooling) was 34.4 °C. The peak temperature is achieved slightly later for 40% N-MPCM, being this peak reached at 36.6 °C by heating cycles.

Table 6*: DSC summary for 20% and 40% N-MPCM pastes: melting/solidification onset, peak temperatures and latent heat storage (average of 3 samples per 3 measurement cycles is reported).*

Mode	***N-MPCM Vol.-%***	***w/b***	***Onset temp. (°C)***	***Peak temp. (°C)***	***Latent heat (J/g)***	***Latent heat (MJ/m^{-3})***
Heating	***20***	***0.45***	*32.8*	*35.3*	*19.08*	*25.42*
		0.40	*32.6*	*35.0*	*18.12*	*26.06*
		0.33	*32.2*	*35.0*	*15.12*	*23.95*
	40	***0.45***	*33.6*	*36.1*	*57.12*	*64.10*
		0.40	*34.1*	*36.6*	*49.94*	*60.98*
		0.33	*34.0*	*36.4*	*45.76*	*56.80*
Cooling	***20***	***0.45***	*34.4*	*32.8*	*16.25*	*-21.65*
		0.40	*34.0*	*32.8*	*15.45*	*-22.22*
		0.33	*34.4*	*32.4*	*12.61*	*-19.97*
	40	***0.45***	*33.3*	*31.5*	*54.73*	*-61.63*
		0.40	*34.4*	*32.3*	*47.01*	*-57.40*
		0.33	*34.4*	*31.9*	*42.45*	*-52.72*

Regarding the effect of the w/b ratio on the enthalpy of the mixtures, there is no big scatter between the conducted average values (*Figure 11*). This result is almost expected since the N-MPCM volume fraction substituted for either 20 Vol.-% or 40 Vol.-% is the same for the different mixtures, independently on the w/b. Therefore, the measured enthalpy is expected to stay constant. These results are also certificating that the casting procedure used will not negatively affect the heat storage potential of the prepared samples. However, a small decreasing trend of mass-specific enthalpy with

decreasing w/b ratio was observed (*Figure 11*), the volumetric amount of Enthalpy presents almost a constant average amount of 20-25 (MJ/m³) for samples with 20% N-MPCM and 55-60 (MJ/m³) for samples with 40% N-MPCM.

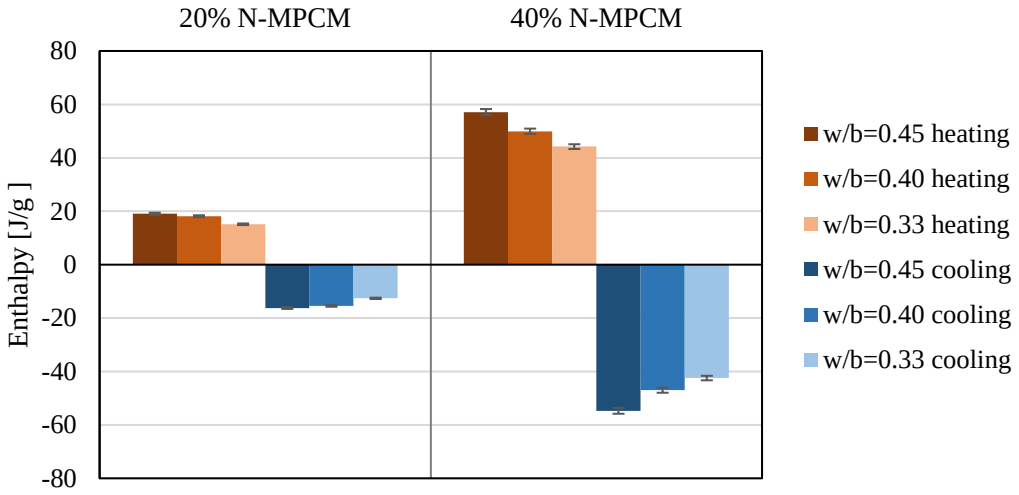

Figure 11: Mass-specific amount of Enthalpy among different paste samples with different w/b ratios for 20% and 40% volumetric amount of N-MPCM.

A higher mass-specific enthalpy was achieved for w/b = 0.45, which is because of the fact that to achieve the same amount of mass between the three w/b ratios, there is a need for more material in the case of w/b=0.45, due to its lower density than w/b=0.33. In other words, there is a slightly higher amount of N-MPCM in 1 g of a sample with w/b = 0.45 than in 1 g of a sample with w/b = 0.33, which leads to a higher enthalpy for the w/b of 0.45.

4.2. Conductivity results

The thermal conductivity of cementitious pastes containing varying amounts of N-MPCM (i.e., 0%, 20% and 40%) was measured using the transient plane source method, commonly known as Hot-Disk. Conductivity values were measured after 28 days of curing time with N-MPCM kept in solid-state (i.e., 10 ºC below and above the melting peak previously measured in DSC tests of the incorporated N-MPCM). The results are shown in *Figure 12*.

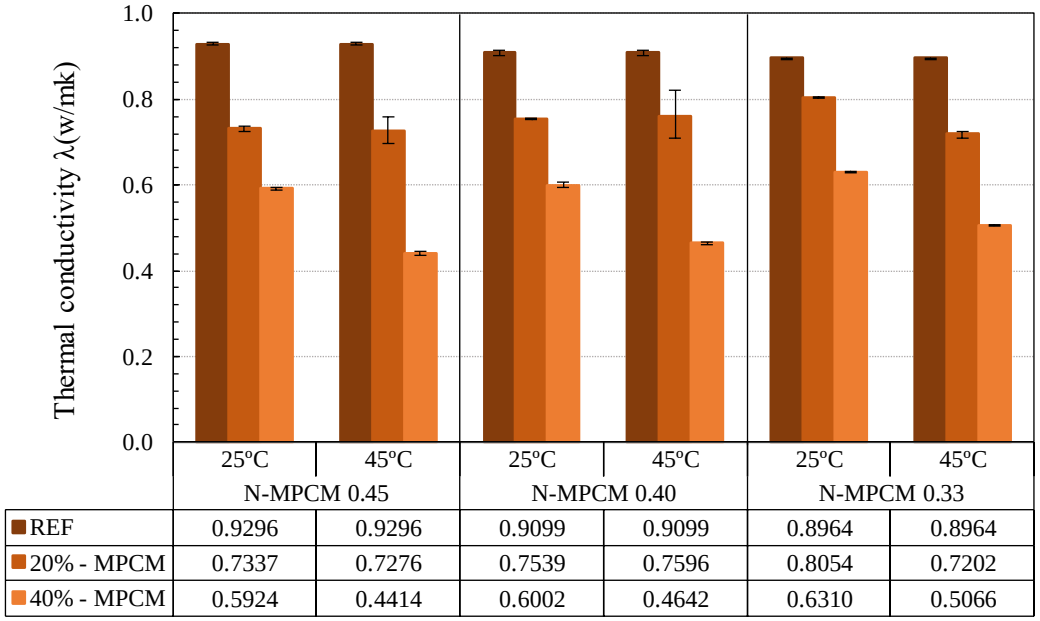

REF	0.9296	0.9296	0.9099	0.9099	0.8964	0.8964
20% - MPCM	0.7337	0.7276	0.7539	0.7596	0.8054	0.7202
40% - MPCM	0.5924	0.4414	0.6002	0.4642	0.6310	0.5066

Figure 12: Thermal conductivities among different w/b ratios for REF, 20% and 40% N-MPCM pastes.

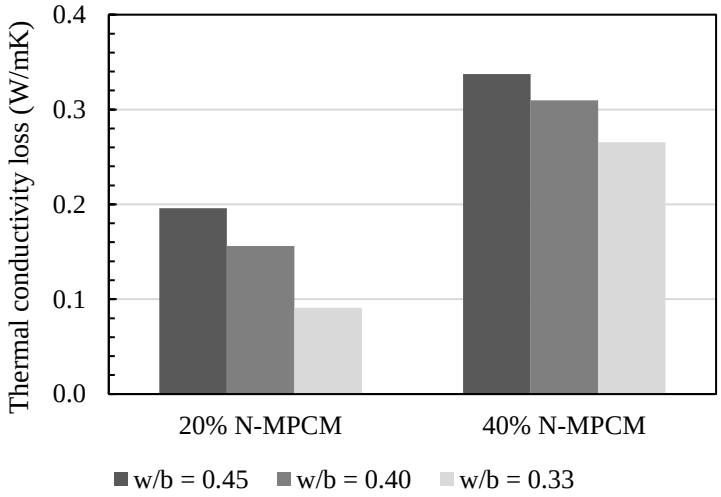

Figure 13: Thermal conductivity loss among different w/b ratios for 20% and 40% N-MPCM pastes.

In all samples with w/b=0.45, 0.40 and 0.33, increasing N-MPCM amounts resulted in a decrease of the thermal conductivity. This is because of the higher thermal conductivity of cement

paste comparing to the N-MPCM which replacement contributes to an overall decrease in the mixture's thermal conductivity. In this sense, *Figure 13* shows the thermal conductivity loss of N-MPCM pastes compared to the reference ones. As general observation, it can be concluded that the decrease of thermal conductivity (W/m×K) is less pronounced in the lower w/b of 0.33, in which the increase of N-MPCM from 20% to 40% contributes to further thermal conductivity decrease (of circa 22%).

4.3. Mechanical tests

4.3.1 Bending tests

Flexural tests were performed for characterizing the bending strengths of the considered N-MPCM pastes. Strength results of each paste, analyzed according to the specifications outlined in Section 4.3, are presented in *Figure 14* and *Figure 15*. From the results it can be observed that the N-MPCM substitution plays a major role on the overall flexural strength reductions. Particularly, this effect is clear and much more dominant for those paste systems, casted with a w/b ratio of 0.33. A remarkable strength loss can be measured when 20% and 40% of N-MPCM volume fractions were substituted, leading to reductions of 23.91% and 48.55% (upon the mean bending strength). The cementitious pastes with a w/b=0.40 and 0.45 showed almost the same trend, but much less evident. The flexural strengths of the REF pastes 0.40 and 0.45 present surprisingly low resistances, probably due to the uncomplete hydration process of the binders (specially the metakaolin ones) and because of early-age cracking due to shrinkage.

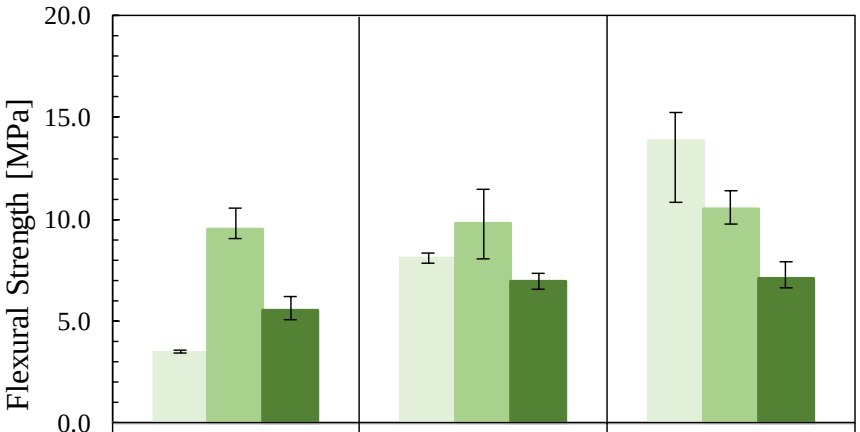

	w/b 0.45	w/b 0.4	w/b 0.33
REF	3.5	8.1	13.8
20% - MPCM	9.5	9.8	10.5
40% - MPCM	5.5	6.9	7.1

Figure 14: 28-days flexural strength values among different w/b ratios and comparing REF, 20% and 40% N-MPCM volume fraction in pastes.

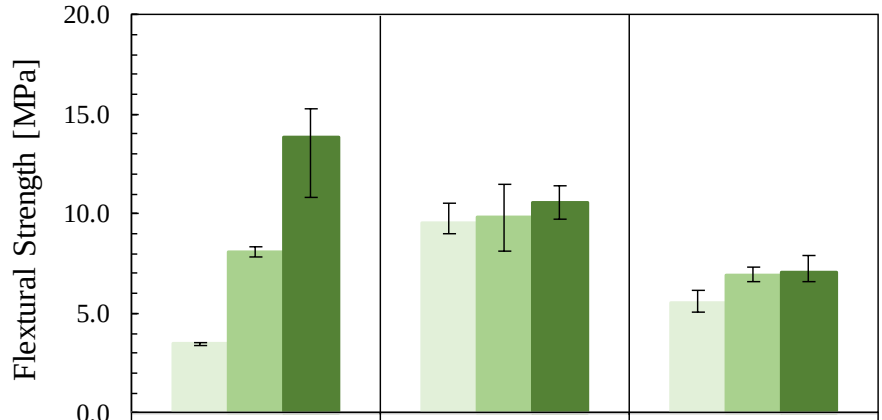

	REF	20% - MPCM	40% - MPCM
w/b 0.45	3.5	9.5	5.5
w/b 0.4	8.1	9.8	6.9
w/b 0.33	13.8	10.5	7.1

494

495 *Figure 15: 28-days flexural strength values among different N-MPCM volume fractions and*
496 *comparing w/b 0.45, w/b 0.40, and w/b 0.33 of pastes.*

497 *Figure 14* and *Figure 15* show the same results, however the first one is aimed at emphasizing
498 the comparative effects of the N-MPCM substitution on the flexural strength, the second on the
499 different w/b ratios. From the latter, it can be observed that bending strengths were strongly
500 influenced by the w/b ratio, meaning: the higher the w/b ratio the lower the corresponding flexural
501 strength. As a matter of fact, this conclusion is quite common for cement-based materials, and the
502 same trend is also followed when the N-MPCM substitutions are considered (see *Figure 15*).
503 However, when higher volumes of N-MPCM are substituted in the cement paste, the flexural strength
504 rise turned out to be much less evident among the mixtures with different w/b ratio. This response
505 can be explained by analyzing the volumetric ratio between the amount of binder and the relative
506 increase of the amount of N-MPCM, which leads to a system that behaves similarly because of the
507 comparable amount of binder. Similar observations were done for the variable w/b ratios and N-
508 MPCM volume substitutions at different maturation times of testing (i.e. 3 days, 7 days and 28 days),
509 as shown in *Figure 16*.

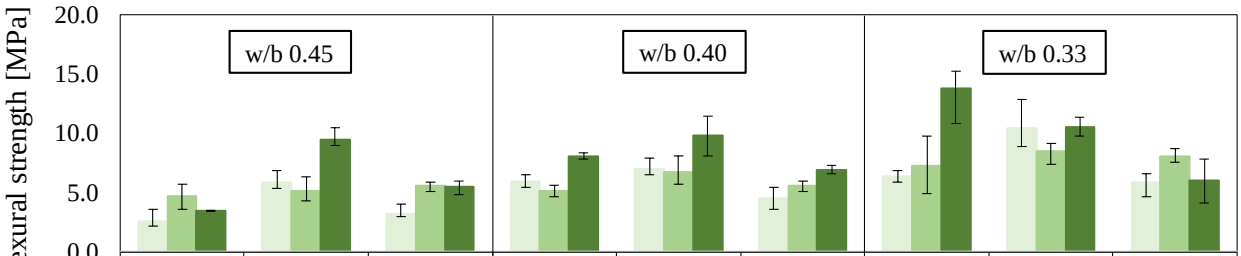

	REF - 0.45	20% - MPCM	40% - MPCM	REF - 0.40	20% - MPCM	40% - MPCM	REF - 0.33	20% - MPCM	40% - MPCM
3 days	2.57	5.87	3.25	5.99	6.98	4.54	6.40	10.46	5.84
7 days	4.69	5.19	5.56	5.19	6.72	5.60	7.24	8.50	8.11
28 days	3.48	9.52	5.51	8.11	9.81	6.93	13.84	10.55	6.04

Figure 16: *Flexural strength values among different w/b ratios, for REF, 20% and 40% N-MPCM pastes and comparing 3, 7 and 28 days of curing time.*

4.3.2 Compressive tests

Compressive strength tests were also performed to investigate the influence of N-MPCM on the mechanical properties of the designed mixtures. The tests were conducted for reference samples, as well as for the samples with volumetric fractions of 20% and 40% N-MPCM. The comparison of the measured compressive strength results at 28 days of curing are presented in *Figure 17* and *Figure 18*, while a full impression of the results, that also considers 3 and 7 days of curing time, are shown in the histograms of *Figure 19*. A first impression reveals that the compressive strength data shows a much more stable and consistent behavior than the bending ones (*Figure 14* to *Figure 16*), while they are also characterized by a much lower scatter. Moreover, the general trend of the compressive strength results shows a consistent strength reduction with either enhancing volume substitution of N-MPCM employed in the system or increasing w/b ratios.

Furthermore, results for the reference pastes show higher compressive strength values for lower w/b ratios. Particularly, the strength increases from REF-0.45 to REF-0.40 is much more pronounced than from REF-0.40 to REF-0.33. In the first case, the rise is +25%, while in the second case, the strength increase is 2.5% only. Moreover, the incorporation of N-MPCM in the cementitious matrix mainly generates a decrease of the compressive strength, independently of the w/b ratio. For example,

529 the substitution of N-MPCM with 20% to 40% generated a further strength loss of approximately
530 50% for each mixture.

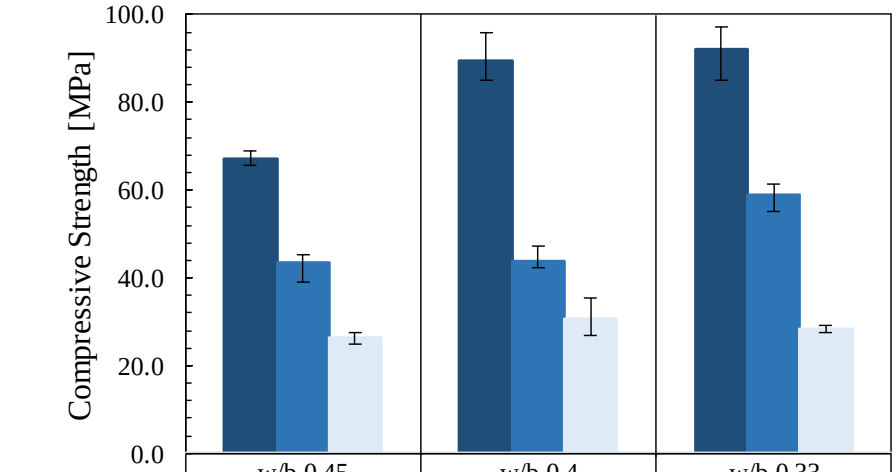

	w/b 0.45	w/b 0.4	w/b 0.33
REF	67.2	89.6	92.2
20% - MPCM	43.4	43.7	58.8
40% - MPCM	26.3	30.5	28.4

531

532 *Figure 17: 28-days compressive strength values among different w/b ratios and comparing REF,*
533 *20% and 40% N-MPCM volume fraction in pastes.*

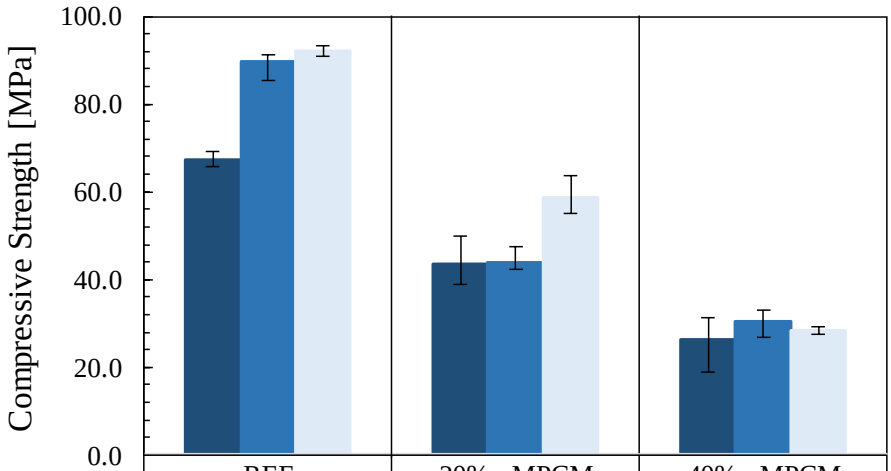

	REF	20% - MPCM	40% - MPCM
w/b 0.45	67.2	43.4	26.3
w/b 0.4	89.6	43.7	30.5
w/b 0.33	92.2	58.8	28.4

534

535 *Figure 18: 28-days compressive strength values among different N-MPCM volume fractions and*
536 *comparing w/b 0.45, w/b 0.40, and w/b 0.33 of pastes.*

The results in *Figure 17* show for a 20% N-MPCM substitution nearly similar results for the w/b ratios of 0.45 and 0.40, while for the w/b ratio of 0.33 a +22% increase in average compressive strength was observed. Moreover, for a 40% N-MPCM substitution, the order of magnitude of the compressive strength values, independently of the w/b ratio, are within the same range, i.e. between 26.3 and 30.5 MPa. When comparing these results with the reference values from *Figure 17*, it can be observed that a 20% N-MPCM substitution leads generally to a reduction of compressive strength: 33% for pastes with a w/b ratio of 0.45, 49% for pastes with a w/b ratio of 0.40 and 36% for pastes with a w/b ratio of 0.33, respectively. Furthermore, the 40% N-MPCM substitution results in an additional 50% strength reduction when compared to the 20% N-MPCM substitution.

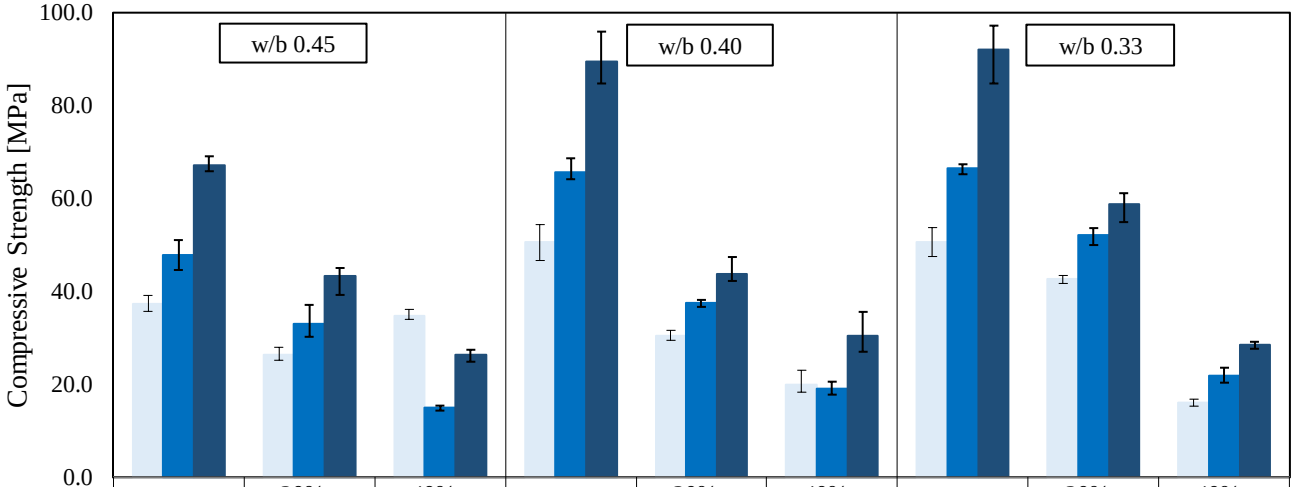

	REF - 0.45	20% - MPCM	40% - MPCM	REF - 0.40	20% - MPCM	40% - MPCM	REF - 0.33	20% - MPCM	40% - MPCM
3 days	37.3	26.4	34.7	50.6	30.5	19.9	50.7	42.7	16.0
7 days	47.8	32.9	14.8	65.8	37.4	19.0	66.5	52.2	21.9
28 days	67.2	43.4	26.3	89.6	43.7	30.5	92.2	58.8	28.4

Figure 19: Compressive strength values among different w/b ratios, for REF, 20% and 40% N-MPCM pastes and comparing 3, 7 and 28 days of curing time.

By analysing *Figure 17* and *Figure 18*, it can be also be observed that the replacement of cement paste by N-MPCM affects the compressive strength considerably more than the change of the w/b ratio. The inherent impact of N-MPCM addition on the mechanical resistance has been also be confirmed by various other authors in literature (see the critical review of [58]). One of the potential

554 reasons for the reduced compressive strength is the increase in porosity due to the N-MPCM addition.
555 This was also stated for instance by Aguayo et al. [59] and was confirmed in this work as well (see
556 Section 4.4).

557 A complete overview of the measured compressive strength data, considering also the different
558 maturation times of testing (i.e., 3 days, 7 days and 28 days), and the three different w/b ratios and
559 N-MPCM volume substitutions, are reported *Figure 19*.

4.4. MIP porosity and pore structure

4.4.1 MIP results

The pore volume of the various cement pastes was determined by MIP tests on samples with a hydration time of 28 days. The effect of w/b ratio on the pore structure with and without N-MPCM addition is measured by means of the change in intruded volume and related pore size distributions. *Figure 20* provides an overview of the results that have been obtained for various mixtures.

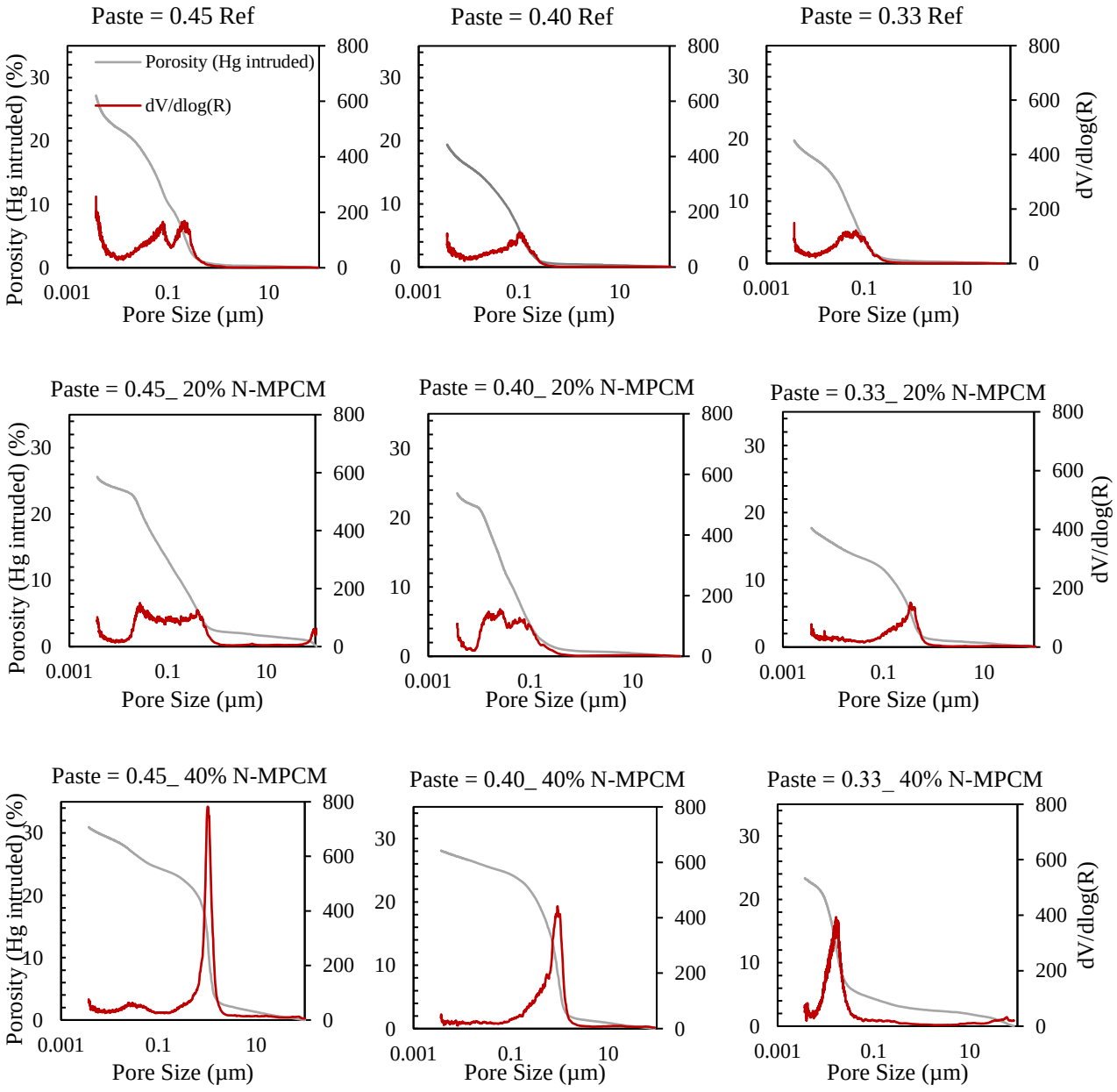

Figure 20: MIP results for REF, 20% and 40% N-MPCM pastes, and for different w/b ratios.

A detailed analysis of the data provided in *Figure 20* reveals that increasing N-MPCM substitutions mainly leads to a higher porosity in the paste structure, indicating that the addition of microcapsules has a significant impact on the pore size/structure of cementitious systems. The latter results in lower mechanical strength and considerably affects heat/moisture transport mechanism through the cementitious system. Furthermore, when w/b decreases, the porosity tends to decrease for all pastes. It is interesting to note that the addition of 40% N-MPCM leads to a more stable pore structure regardless of the w/b ratio. In contrast, a much wider pore size distribution is seen for 20% N-MPCM. The critical pore size is clear for the case of 40% N-MPCM; however, the w/b appears to have a significant effect on the pore size of the system with w/b of 0.45 and 0.40, being very similar to each other and 0.33 being much lower. This is mainly because of the poor interface bond between the N-MPCM-shell and the cementitious matrix, especially for higher w/b ratios and also because of the hydrophobic nature of the N-MPCM capsules, which will repel the water and cause air gaps between shell surface and cementitious matrix. An overview of the achieved results is given in Table 7.

Table 7*: Overview of the sample porosities and critical pore diameter measurements via MIP.*

	w/b = 0.45			***w/b = 0.40***			***w/b = 0.33***		
	Ref	***20%***	***40%***	***Ref***	***20%***	***40%***	***Ref***	***20%***	***40%***
Critical pore diameter (µm)	*0.236*	*0.029*	*1.050*	*0.105*	*0.025*	*0.912*	*0.076*	*0.359*	*0.018*
Intrudable porosity (%)	*24.22*	*25.62*	***30.97***	*20.40*	*23.54*	*28.11*	*18.84*	***17.73***	*23.36*

Among all prepared samples, the highest porosity (30.97 %) is measured for the mixtures with 40% N-MPCM and w/b=0.45, and the lowest porosity (17.73 %) for the samples with 20% N-MPCM and a w/b ratio of 0.33. The results indicate that the phenomena that may affect the porosity of cement paste with N-MPCM included, can be various. Firstly, the size of single microcapsules which might

591 fill the cavities between the hydrating cementitious particles, leading to improved particle packing
592 density and a decreasing porosity (see also [57]). This effect can also explain the lower porosity for
593 samples with 20% N-MPCM and a w/b ratio of 0.33, when compared with the Ref-0.33. On the
594 contrary, the hydrophobic nature of N-MPCM may contribute to a higher porosity as well. When
595 microcapsules are added to a mixture, they tend to repel water, so air bubbles may adhere to a
596 microcapsule, resulting in higher porosity in the cement paste mixtures. A third possible effect is the
597 agglomeration of microcapsules in the cementitious system, which avoids an optimum packing
598 density, and finally results in a higher porosity. The porosity of N-MPCM-enhanced cementitious
599 systems can be explained and evaluated by a combined effect of these three possible causes.

600 *4.4.2 Dependency between porosity, strength and thermal properties*

601 The dependency between the compressive strength (Section 4.3) and the porosity is elaborated
602 in *Figure 21*-a for the various cement based mixtures with different w/b ratios and N-MPCM
603 volumetric amounts. The results show a clear linear trend with the porosity dominated by either the
604 w/b ratio or the volumetric amount of N-MPCM. In this sense, it can be observed that the lowest
605 compressive strength belongs to samples with 40% volumetric amount of N-MPCM which are clearly
606 dominated by the highest porosity, and mainly affected by the % of cement paste replaced by N-
607 MPCM.

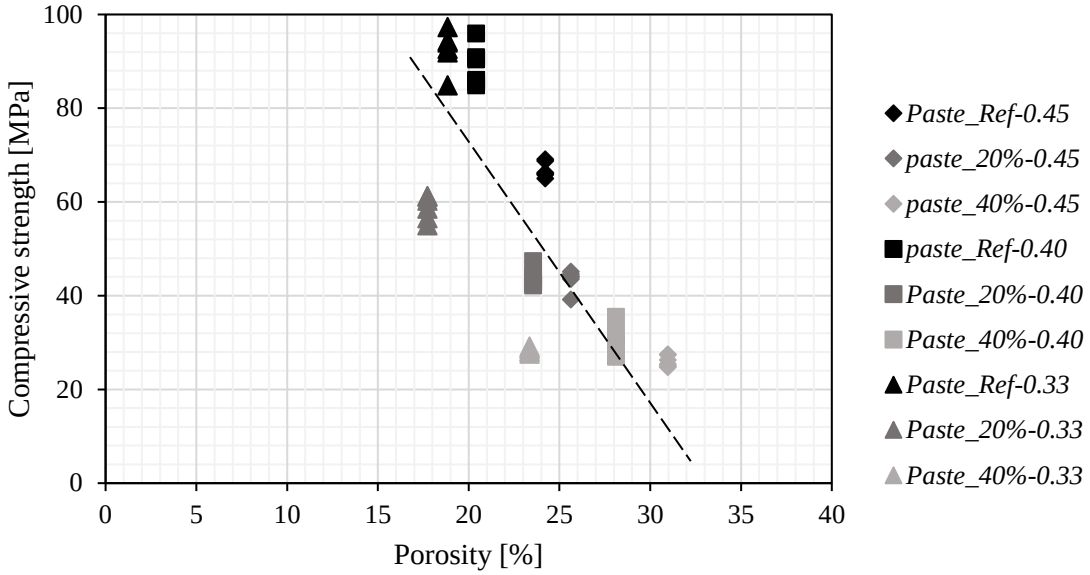

608

609 (a)

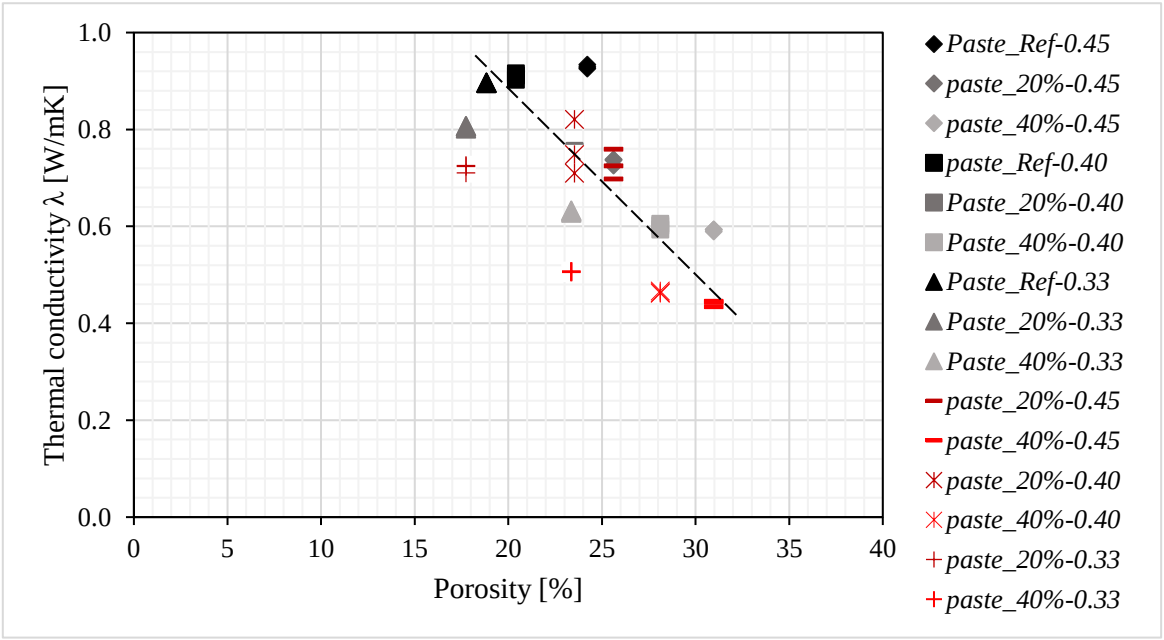

610

611 (b)

612 *Figure 21: a) Compressive strength vs porosity and b) Thermal Conductivity vs porosity of REF,*

613 *20% and 40% N-MPCM-cement pastes. Black/grey points show the measured conductivity by 25 °C*

614 *and red points show the measured conductivity by 45°C.*

615 From *Figure 21*-b, a clear relationship between the thermal conductivity and porosity of the

616 various cementitious mixtures can be observed. This also implicitly indicates a dependency between

617 the compressive strength and the thermal conductivity. The change in porous microstructure of N-

MPCM-cementitious systems is thus directly linked to a change in thermal conductivity, or to a change of the compressive strength. These results reveal the important role that the inner pores (amount and structure) play especially when optimum thermal, mechanical and/or TES properties are considered.

From the results shown in *Figure 21*, it is evident that the pastes with the same % of N-MPCM are characterized to have a very similar thermal conductivity, independently of the w/b ratio.

4.5. Morphological and elemental analysis via SEM

The morphological analysis of the sample surfaces was investigated with a SEM characterization technique with the aim to study the N-MPCM microcapsules and their integrity in cement paste microstructures. The results are presented in this section.

4.5.1 Reference pastes

Figure 22 provides the microstructure of the various cementitious paste samples without N-MPCM, indicating the effect of the employed w/b ratios on the microstructure morphology. The presence of micro cracks caused by hardening shrinkage is evident for all samples. In all mixtures, the dispersion of a lighter phase (blue arrow) and a slightly darker phase (yellow arrow), indicate the various binder material in the cementitious system. To identify the composition of these phases, an elemental analysis with EDS was performed as shown in *Figure 23*.

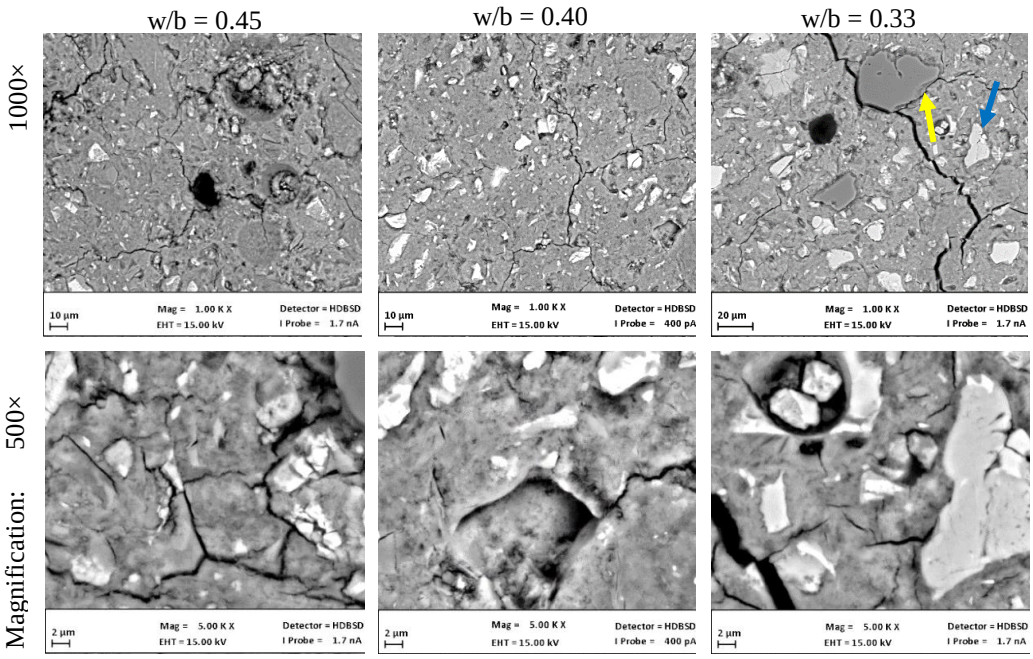

635

636 *Figure 22: SEM micrographs of the reference pastes and considering different w/b ratios.*

637

638

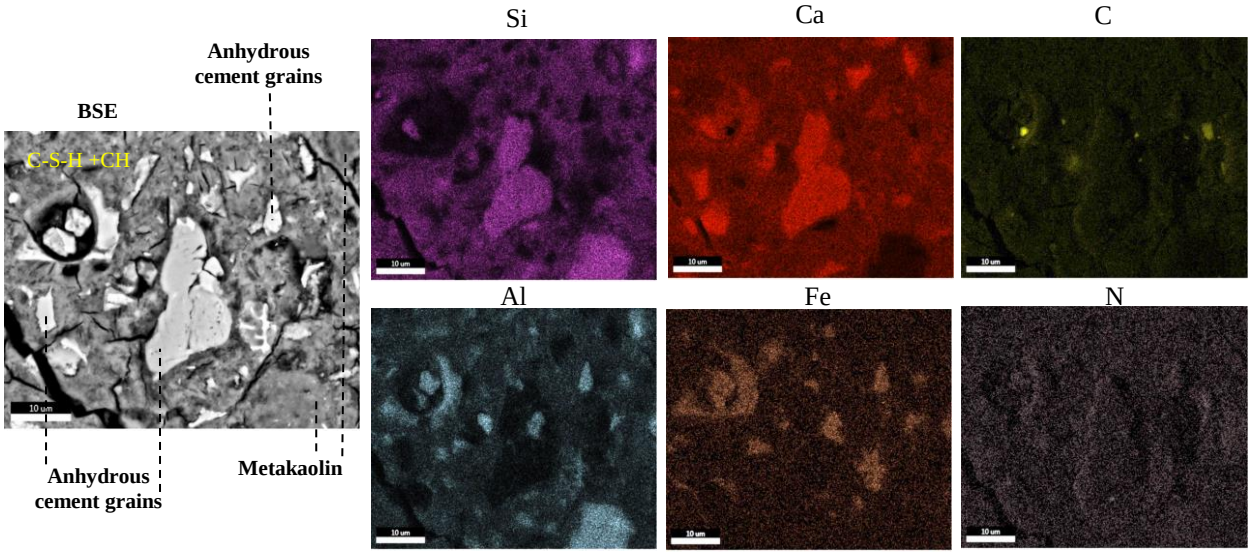

639

640 *Figure 23: SEM-EDS mapping of the w/b=0.33 reference pastes providing the distribution of*

641 *chemical components available in the composite.*

With consideration of the chemical composition of cement and metakaolin provided in Section 2.1, the obtained EDS maps can be employed to characterize the individual elements. Firstly, the lighter phases are associated with anhydrous cement elements, represented by higher concentrations of calcium (Ca) and silica (Si). Secondly, the concentration of iron (Fe) confirms further anhydrous hydration products (more precisely, ferrite), indicated by a slightly brighter color. Lastly, the presence of both silica (Si) and aluminum (Al), indicate the presence of metakaolin that contains both these elements. The rest of the paste contains various hydration products among which C-S-H and CH.

Moreover, when considering the expected chemical composition of N-MPCM with a polymeric shell (made from the polymerization of formaldehyde, with the chemical formula CH2O, and melamine with the chemical formula C3H6N6), the presence of carbon (C) and nitrogen (N) was also examined.

Since the N-MPCM contains carbon in its shell composition, it is not recommended to treat the surface of N-MPCM-composite with the epoxy impregnation technique to simplify N-MPCM detection. Finally, small amounts of distributed nitrogen were also observed that can most likely be attributed to the SEM N-filled vacuum chamber.

4.5.2 Elemental analysis of N-MPCM in the cementitious matrix

An EDS analysis was carried out for the N-MPCM pastes, where *Figure 24* shows the evaluation of the N-MPCM distribution in the cement paste. The Figure only shows the micrographs for a w/b ratio of 0.33 and 0.45, both with a 40% N-MPCM content. The full elementary analysis confirmed a similar distribution for all cases.

The SEM micrographs show an equally distribution of the N-MPCM in the cement-paste matrix (indicated in *Figure 24*). It can also be observed that the microcracks propagate mostly across the spherical voids without harming N-MPCM microcapsules. The soft organic polymer shell of the N-MPCM microcapsule clearly presents the weakest element among the inorganic constituents inside the cement-paste matrices. In this sense, these N-MPCM particles act as a crack initiator.

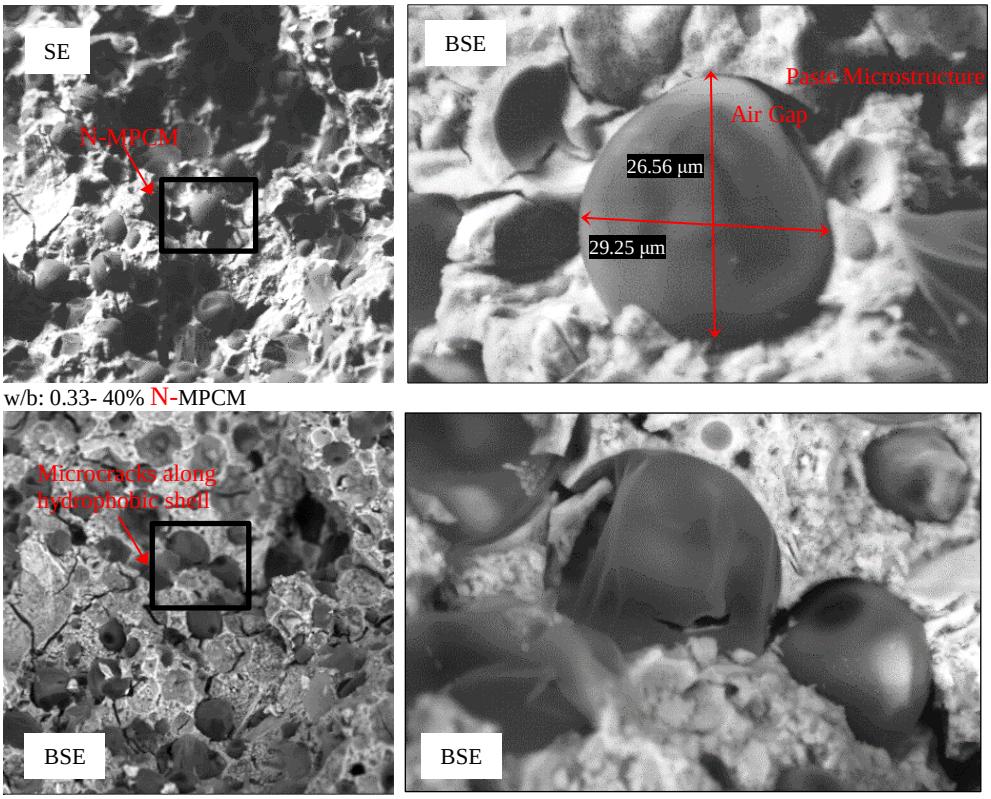

Figure 24 SEM micrograph of N-MPCM for a w/b ratio of 0.33 and 0.45, both with a 40% N-MPCM content in the paste. The amplification shows detailed views of the N-MPCM distribution in the cement paste matrix.

A closer look on the compatibility of the cement matrix with N-MPCM reveals the presence of possible gaps between the shell interface and the cement-paste matrices. The hydrophobic nature of N-MPCM shell, which repels water, cause the air entrapment between the capsules and the cement paste.

By using the BSE detector for the same spot and magnification as the SE detector, more information on the presence of N-MPCM could be obtained for unpolished samples. As one of the goals was to determine the state of the capsule, the BSE detector was used to take a closer look at 5000× of magnification.

N-MPCM appearance was partly affected by the polishing treatment to prepare samples for SEM-EDS analysis. In contrast, the shape and adhesion of the N-MPCM to the matrix, as well as the presence of a crack in a shell, were easier to identify in unpolished samples. As a result, the SEM-

EDS study on the N-MPCM-composites was conducted on unpolished samples as shown in *Figure 24*.

The evaluation of the element composition for a N-MPCM capsule was also performed. *Figure 25* shows the element mapping of N-MPCM, which provides a back-scattered image (BSE) and a graphical distribution of the analyzed chemical elements i.e., Carbon (C) and Nitrogen (N). The SEM analysis of the N-MPCM particles, embedded in the cement paste matrix, confirms the presence of a single capsule by its high concentration of both carbon (C) and nitrogen (N).

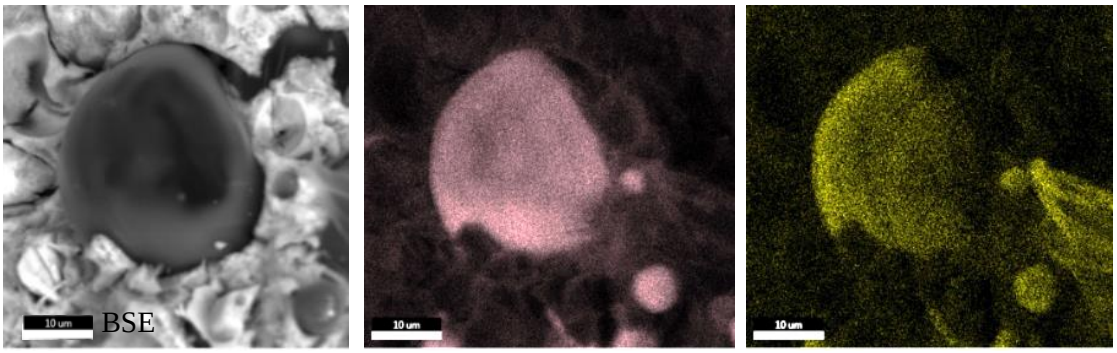

Figure 25: SEM-EDS mapping of the N-MPCM providing a detailed back-scattered image (BSE), a distribution of carbon (C) and nitrogen (N).

The relationship between the amounts of each compound can be compared and evaluated based on the amount of oxides present. Therefore, the calculated chemical composition for the polymer shell based on the C/O ratio is 0.847, compared to the ratio of 0.179 for N/O. This reveals that the shell is mainly composed of carbon with a smaller amount of nitrogen, which complies with the basic formulation of melamine-formaldehyde ($C_3H_6N_6$).

5. CONCLUSIONS

This work is reporting the results and analysis of an extensive experimental study on cement paste enhanced with Nextek 37D®-Microencapsulated Phase Change Materials (N-MPCM) for Thermal Energy Storage (TES) purposes. Three different water-to-binder ratios (0.45, 0.40 and 0.33) and two N-MPCM volume fractions (20% and 40%, plus a 0% reference mix) were investigated.

Based on the experimental results, the following conclusions can be drawn:

- Particle size of N-MPCM was investigated through size diffractometer measurements which indicated a mean particle size of 20.9 μm, with a low tendency to agglomerate.
- The wettability of the N-MPCM was assessed via contact angle measurements. The test was performed with 10 times repetitions and results showed an average contact angle of 110.7 º, confirming the hydrophobic nature of the considered microcapsules.
- DSC-measurements on N-MPCM were conducted with a heating/cooling rate of 0.5 $K \times min^{-1}$. The experimental data showed a melting peak temperature of 36.5 °C, and 31.7 °C for the solidification one. The latent heat was 197.3 J/g and 194.6 J/g for heating and cooling, respectively.
- DSC results of the composites (i.e., REF pastes and MPMC pastes) showed an almost similar sensible heat capacity for the cement pastes with different w/b ratios and without N-MPCM. For the pastes enhanced with N-MPCM substitutions, evident latent peaks were recorded in the temperature region where the phase change occurred (either in melting or solidification stage). The volumetric latent enthalpies showed an almost constant average of 20-25 (MJ/m^3) for samples with 20% N-MPCM and 55-60 (MJ/m^3) for samples with 40% N-MPCM, independent of the w/b ratio.
- Thermal conductivities were studied by Hot-Disk measurements to assess the influence of the w/b ratio and the amount of MPMC substituted. The experimental results showed a decreasing thermal conductivity for higher w/b ratios and/or when the N-MPCM volume fractions are

724 higher. Thermal conductivity values were measured at 25 and 45 °C which values ranged
725 between 0.93 to 0.44 W/m×K: N-MPCM amounts and w/b ratios play the major roles in the
726 conductivity loss.

727 • Compressive and bending tests, conducted at different times of hydration, showed a strength
728 loss trend which can be due to either increasing w/b ratio and/or increasing amount of N-
729 MPCM substitution. Strength loss due to N-MPCM addition could be explained by several
730 concurring factors such as the low mechanical strength of N-MPCM shells, the weak interface
731 bond strength between the cement matrix and N-MPCM, and the increase of the porosity of
732 the N-MPCM-cement paste matrix.

733 • MIP tests were performed to characterize the pore structure after 28 days of hydration. Pore
734 size distribution and total intruded porosity, for different w/b ratios and volumetric amount of
735 N-MPCM, were investigated. The results showed that an increase of the N-MPCM
736 substitutions lead to a higher porosity in the cement paste. Moreover, the w/b ratio also
737 showed a significant effect on the pore size distribution of all tested cement paste systems.
738 The highest porosity (30.97 %) was measured for the mixture with 40% N-MPCM and a
739 w/b=0.45, while the lowest porosity (17.73 %) was measured on samples with 20% N-MPCM
740 and a w/b of 0.33.

741 • Scanning Electron Microscopy (SEM) analyses was performed to investigate the microscopic
742 properties and to examine the distribution of chemical components (via SEM-EDS) present in the
743 ~~cement~~ paste matrix. Chemical compositions, geometry, shape, particle size, and particle
744 distribution were investigated for both plain cement paste and N-MPCM-paste systems. The
745 results showed a homogeneous distribution of N-MPCM, a proper shell integrity, envisioned
746 various particle sizes and uniformity of microcapsules, confirmed mechanical stability and gave
747 a clear impression N-MPCM have on the microstructure morphology and chemistry of the
748 cementitious composites.

This extensive experimental study can be considered as a first step towards the development of multiscale numerical model for analyzing the TES behavior of N-MPCM-based cementitious composites. Furthermore, numerical developments, including lower scale observations (i.e., nano-, micro- and meso-scales) for capturing local effects of the porous network, such as MPMC, air bubbles, interfaces, cracks, etc., plus building energy simulations, are currently ongoing while aiming to optimize and design various model parameters, without the need of performing time-demanding experimental tests.

ACKNOWLEDGEMENTS

This work is part of the research activities of the NRG-STORAGE project (GA 870114, https://nrg-storage.eu/, accesses verified on 18 November 2021), financed by the European Union H2020 Framework under the LC-EEB-01-2019 call, H2020-NMBP-ST-IND-2018-2020/H2020-NMBP-EEB-2019, IA type. The support provided by EU H2020-NRG-STORAGE is gratefully acknowledged.

REFERENCES

[1] Tian, C., Feng, G., Li, S., & Xu, F. (2019). Scenario analysis on energy consumption and CO2 emissions reduction potential in building heating sector at community level. Sustainability, 11(19), 5392.

[2] Heating and cooling | EASME, https://ec.europa.eu/easme/en/section/horizon-2020-energy-efficiency/heating-and cooling#inline-nav-1, last accessed 28/04/2021.

[3] Ürge-Vorsatz, D., Cabeza, L. F., Serrano, S., Barreneche, C., & Petrichenko, K. (2015). Heating and cooling energy trends and drivers in buildings. Renewable and Sustainable Energy Reviews, 41, 85-98.

[4] https://ec.europa.eu/info/strategy/priorities-2019-2024/european-green-deal_en

[5] Baniasadi, A., Habibi, D., Al-Saedi, W., Masoum, M. A., Das, C. K., & Mousavi, N. (2020). Optimal sizing design and operation of electrical and thermal energy storage systems in smart buildings. Journal of Energy Storage, 28, 101186.

[6] Tang, R., & Wang, S. (2019). Model predictive control for thermal energy storage and thermal comfort optimization of building demand response in smart grids. Applied Energy, 242, 873-882.

[7] Zavrl, E., & Stritih, U. (2019). Improved thermal energy storage for nearly zero energy buildings with PCM integration. Solar energy, 190, 420-426.

[8] Tyagi, V. V., Chopra, K., Kalidasan, B., Chauhan, A., Stritih, U., Anand, S., ... & Kothari, R. (2021). Phase change material based advance solar thermal energy storage systems for building heating and cooling applications: A prospective research approach. Sustainable Energy Technologies and Assessments, 47, 101318.

[9] Gholamibozanjani, G., & Farid, M. (2020). A comparison between passive and active PCM systems applied to buildings. Renewable Energy, 162, 112-123.

[10] Saxena, R., Rakshit, D., & Kaushik, S. C. (2020). Experimental assessment of Phase Change Material (PCM) embedded bricks for passive conditioning in buildings. Renewable Energy, 149, 587-599.

[11] Maleki, B., Khadang, A., Maddah, H., Alizadeh, M., Kazemian, A., & Ali, H. M. (2020). Development and thermal performance of nanoencapsulated PCM/plaster wallboard for thermal energy storage in buildings. Journal of Building Engineering, 32, 101727.

[12] Bentz, D. P., Peltz, M. A., Duran-Herrera, A., Valdez, P., & Juarez, C. A. (2011). Thermal properties of high-volume fly ash mortars and concretes. Journal of Building Physics, 34(3), 263-275.

[13] Srinivasaraonaik, B., Sinha, S., & Singh, L. P. (2021). Synthesis of encapsulation of binary mixture by silica and its performance in pure cementitious system. Energy Storage, 3(3), e229.

[14] Nazari Sam, M., Caggiano, A., Mankel, C., & Koenders, E. (2020). A comparative study on the thermal energy storage performance of bio-based and paraffin-based PCMs using DSC procedures. Materials, 13(7), 1705.

[15] Stritih, U., Tyagi, V. V., Stropnik, R., Paksoy, H., Haghighat, F., & Joybari, M. M. (2018). Integration of passive PCM technologies for net-zero energy buildings. Sustainable cities and society, 41, 286-295.

[16] Lin, Y., Jia, Y., Alva, G., & Fang, G. (2018). Review on thermal conductivity enhancement, thermal properties and applications of phase change materials in thermal energy storage. Renewable and sustainable energy reviews, 82, 2730-2742.

[17] Pandey, A. K., Hossain, M. S., Tyagi, V. V., Abd Rahim, N., Jeyraj, A., Selvaraj, L., & Sari, A. (2018). Novel approaches and recent developments on potential applications of phase change materials in solar energy. Renewable and Sustainable Energy Reviews, 82, 281-323.^

[18] Tyagi, V. V., Chopra, K., Sharma, R. K., Pandey, A. K., Tyagi, S. K., Ahmad, M. S., ... & Kothari, R. (2022). A comprehensive review on phase change materials for heat storage

applications: Development, characterization, thermal and chemical stability. Solar Energy Materials and Solar Cells, 234, 111392.

[19] Ramakrishnan, S., Sanjayan, J., Wang, X., Alam, M., & Wilson, J. (2015). A novel paraffin/expanded perlite composite phase change material for prevention of PCM leakage in cementitious composites. Applied Energy, 157, 85-94.

[20] Hawlader, M. N. A., Uddin, M. S., & Khin, M. M. (2003). Microencapsulated PCM thermal-energy storage system. Applied energy, 74(1-2), 195-202.

[21] Konuklu, Y., Ostry, M., Paksoy, H. O., & Charvat, P. (2015). Review on using microencapsulated phase change materials (PCM) in building applications. Energy and Buildings, 106, 134-155.

[22] Regin, A. F., Solanki, S. C., & Saini, J. S. (2009). An analysis of a packed bed latent heat thermal energy storage system using PCM capsules: Numerical investigation. Renewable energy, 34(7), 1765-1773.

[23] Adesina, A. (2019). Use of phase change materials in concrete: current challenges. Renewable Energy and Environmental Sustainability, 4, 9.

[24] Hawlader, M. N. A., Uddin, M. S., & Khin, M. M. (2003). Microencapsulated PCM thermal-energy storage system. Applied energy, 74(1-2), 195-202.

[25] Farid, M. M., Khudhair, A. M., Razack, S. A. K., & Al-Hallaj, S. (2004). A review on phase change energy storage: materials and applications. Energy conversion and management, 45(9-10), 1597-1615.

[26] Ren, M., Wen, X., Gao, X., & Liu, Y. (2021). Thermal and mechanical properties of ultra-high performance concrete incorporated with microencapsulated phase change material. Construction and Building Materials, 273, 121714.

[27] Ricklefs, A., Thiele, A. M., Falzone, G., Sant, G., & Pilon, L. (2017). Thermal conductivity of cementitious composites containing microencapsulated phase change materials. International journal of heat and mass transfer, 104, 71-82.

[28] Mankel, C., Caggiano, A., Ukrainczyk, N., & Koenders, E. (2019). Thermal energy storage characterization of cement-based systems containing microencapsulated-PCMs. Construction and Building Materials, 199, 307-320.

[29] Gencel, O., Yaras, A., Hekimoğlu, G., Ustaoglu, A., Erdogmus, E., Sutcu, M., & Sarı, A. (2022). Cement based-thermal energy storage mortar including blast furnace slag/capric acid shape-stabilized phase change material: Physical, mechanical, thermal properties and solar thermoregulation performance. Energy and Buildings, 111849.

[30] Hekimoğlu, G., Nas, M., Ouikhalfan, M., Sarı, A., Kurbetci, Ş., Tyagi, V. V., ... & Saleh, T. A. (2021). Thermal management performance and mechanical properties of a novel cementitious composite containing fly ash/lauric acid-myristic acid as form-stable phase change material. Construction and Building Materials, 274, 122105.

[31] Sarı, A., Hekimoğlu, G., Tyagi, V. V., & Sharma, R. K. (2020). Evaluation of pumice for development of low-cost and energy-efficient composite phase change materials and lab-scale thermoregulation performances of its cementitious plasters. Energy, 207, 118242.

[32] Sarı, A., Bicer, A., Karaipekli, A., & Al-Sulaiman, F. A. (2018). Preparation, characterization and thermal regulation performance of cement based-composite phase change material. Solar energy materials and solar cells, 174, 523-529.

[33] Amran, Y. M., Farzadnia, N., & Ali, A. A. (2015). Properties and applications of foamed concrete; a review. Construction and Building Materials, 101, 990-1005.

[34] Xu, B., & Li, Z. (2013). Paraffin/diatomite composite phase change material incorporated cement-based composite for thermal energy storage. Applied energy, 105, 229-237.

[35] Ramakrishnan, S., Sanjayan, J., Wang, X., Alam, M., & Wilson, J. (2015). A novel paraffin/expanded perlite composite phase change material for prevention of PCM leakage in cementitious composites. Applied Energy, 157, 85-94.

[36] Rathore, P. K. S., Shukla, S. K., & Gupta, N. K. (2020). Potential of microencapsulated PCM for energy savings in buildings: A critical review. Sustainable Cities and Society, 53, 101884.

[37] Lu, S., Li, Y., Kong, X., Pang, B., Chen, Y., Zheng, S., & Sun, L. (2017). A review of PCM energy storage technology used in buildings for the global warming solution. Energy Solutions to Combat Global Warming, 611-644.

[38] Snoeck, D., Priem, B., Dubruel, P., & De Belie, N. (2016). Encapsulated Phase-Change Materials as additives in cementitious materials to promote thermal comfort in concrete constructions. Materials and structures, 49(1), 225-239.

[39] Aguado, A., Fernández, A. I., Cabeza, L. F., & Chimenos, J. M. (2014). Review of the use of phase change materials (PCMs) in buildings with reinforced concrete structures. Mater. Construcc, 64(315), e031.

[40] Cao, V. D., Pilehvar, S., Salas-Bringas, C., Szczotok, A. M., Do, N. B. D., Le, H. T., ... & Kjøniksen, A. L. (2018). Influence of microcapsule size and shell polarity on the time-dependent viscosity of geopolymer paste. Industrial & Engineering Chemistry Research, 57(29), 9457-9464.

[41] Coppola, L., Coffetti, D., & Lorenzi, S. (2016). Cement-based renders manufactured with phase-change materials: applications and feasibility. Advances in Materials Science and Engineering, 2016.

[42] Sanfelix, S. G., Santacruz, I., Szczotok, A. M., Belloc, L. M. O., Angeles, G., & Kjøniksen, A. L. (2019). Effect of microencapsulated phase change materials on the flow behavior of cement composites. Construction and Building Materials, 202, 353-362.

[43] Meshgin, P., & Xi, Y. (2012). Effect of Phase-Change Materials on Properties of Concrete. ACI Materials Journal, 109(1).

[44] Dehdezi, P. K., Hall, M. R., Dawson, A. R., & Casey, S. P. (2013). Thermal, mechanical and microstructural analysis of concrete containing microencapsulated phase change materials. International Journal of Pavement Engineering, 14(5), 449-462.

[45] Fernandes, F., Manari, S., Aguayo, M., Santos, K., Oey, T., Wei, Z., ... & Sant, G. (2014). On the feasibility of using phase change materials (PCMs) to mitigate thermal cracking in cementitious materials. Cement and Concrete Composites, 51, 14-26.

[46] PN-EN 197-1 "Cement. Part 1. Composition, specifications and conformity criteria for common cements".

[47] Centrilit NC II Concrete Additive Based on Pozzolanic Alumosilicate, https://www.mc-bauchemie.hr/docs/technical/Centrilit_NC_II.pdf

[48] Microtech Laborathories, 2019. [Online]. Available: https://www.microteklabs.com/nextek-37d.

[49] EN 196-1, 'Methods of Testing Cement – Part 1: Determination of Strength', (2005).

[50] Liu, X., Hu, S., Tang, Y., Xie, Z., Liu, J., & He, Y. (2020). Selecting a proper microsphere to combine optical trapping with microsphere-assisted microscopy. Applied Sciences, 10(9), 3127.

[51] Hebbar, R. S., Isloor, A. M., & Ismail, A. F. (2017). Contact angle measurements. In Membrane characterization (pp. 219-255). Elsevier.

[52] DIN 51005. 2005. Thermal analysis (TA) - Terms.

[53] DIN 51007. 2019. Thermal analysis – Differential thermal analysis (DTA) and differential scanning calorimetry (DSC) –General Principles.

[54] IEA-SHC 42 / ECES Annex 29. 2015. Standard to determine the heat storage capacity of PCM using hf-DSC with constant heating/cooling rate (dynamic mode). A technical report of subtask A2.1.

[55] International Standard, "Pore size distribution and porosity of solid materials by mercury porosimetry and gas adsorption. Mercury Porosimetry (ISO 15901)," ISO 15901, 2006.

[56] Anovitz, L. M., & Cole, D. R. (2015). Characterization and analysis of porosity and pore structures. Reviews in Mineralogy and geochemistry, 80(1), 61-164.

[57] Cao, V. D., Pilehvar, S., Salas-Bringas, C., Szczotok, A. M., Rodriguez, J. F., Carmona, M., ... & Kjøniksen, A. L. (2017). Microencapsulated phase change materials for enhancing the thermal performance of Portland cement concrete and geopolymer concrete for passive building applications. Energy Conversion and Management, 133, 56-66.

[58] Marani, A., & Nehdi, M. L. (2019). Integrating phase change materials in construction materials: Critical review. Construction and Building Materials, 217, 36-49.

[59] Aguayo, M., Das, S., Maroli, A., Kabay, N., Mertens, J. C., Rajan, S. D., ... & Neithalath, N. (2016). The influence of microencapsulated phase change material (PCM) characteristics on the microstructure and strength of cementitious composites: Experiments and finite element simulations. Cement and Concrete Composites, 73, 29-41.